Dendritic cell paucity in mismatch repair–proficient colorectal cancer liver metastases limits immune checkpoint blockade efficacy

William W. Ho[a,b,1], Igor L. Gomes-Santos[a], Shuichi Aoki[a,2], Meenal Datta[a], Kosuke Kawaguchi[a,3], Nilesh P. Talele[a], Sylvie Roberge[a], Jun Ren[a], Hao Liu[a,4], Ivy X. Chen[a], Patrik Andersson[a], Sampurna Chatterjee[a], Ashwin S. Kumar[a,c], Zohreh Amoozgar[a], Qixian Zhang[a], Peigen Huang[a], Mei Rosa Ng[a], Vikash P. Chauhan[a,5], Lei Xu[a], Dan G. Duda[a], Jeffrey W. Clark[d], Mikael J. Pittet[e,f,g,h,6], Dai Fukumura[a,6], and Rakesh K. Jain[a,6]

[a]Edwin L. Steele Laboratories, Department of Radiation Oncology, Massachusetts General Hospital and Harvard Medical School, Boston, MA 02114; [b]Department of Chemical Engineering, Massachusetts Institute of Technology, Cambridge, MA 02139; [c]Harvard–MIT Program in Health Sciences and Technology, Massachusetts Institute of Technology, Cambridge, MA 02139; [d]Department of Hematology/Oncology, Massachusetts General Hospital and Harvard Medical School, Boston, MA 02114; [e]Department of Pathology and Immunology, University of Geneva, CH-1211 Geneva, Switzerland; [f]Ludwig Institute for Cancer Research, 1005 Lausanne, Switzerland; [g]Department of Oncology, Geneva University Hospitals, CH-1211 Geneva, Switzerland; and [h]Center for Systems Biology, Massachusetts General Hospital and Harvard Medical School, Boston, MA 02114

Contributed by Rakesh K. Jain, September 1, 2021 (sent for review March 19, 2021; reviewed by David DeNardo and Megan Ruhland)

Liver metastasis is a major cause of mortality for patients with colorectal cancer (CRC). Mismatch repair–proficient (pMMR) CRCs make up about 95% of metastatic CRCs, and are unresponsive to immune checkpoint blockade (ICB) therapy. Here we show that mouse models of orthotopic pMMR CRC liver metastasis accurately recapitulate the inefficacy of ICB therapy in patients, whereas the same pMMR CRC tumors are sensitive to ICB therapy when grown subcutaneously. To reveal local, nonmalignant components that determine CRC sensitivity to treatment, we compared the microenvironments of pMMR CRC cells grown as liver metastases and subcutaneous tumors. We found a paucity of both activated T cells and dendritic cells in ICB-treated orthotopic liver metastases, when compared with their subcutaneous tumor counterparts. Furthermore, treatment with Feline McDonough sarcoma (FMS)-like tyrosine kinase 3 ligand (Flt3L) plus ICB therapy increased dendritic cell infiltration into pMMR CRC liver metastases and improved mouse survival. Lastly, we show that human CRC liver metastases and microsatellite stable (MSS) primary CRC have a similar paucity of T cells and dendritic cells. These studies indicate that orthotopic tumor models, but not subcutaneous models, should be used to guide human clinical trials. Our findings also posit dendritic cells as antitumor components that can increase the efficacy of immunotherapies against pMMR CRC.

immune checkpoint blockade | cancer immunotherapy | tumor immune microenvironment | mismatch repair–proficient colorectal cancer | orthotopic tumor model

Significance

Immune checkpoint blockade (ICB) has been efficacious in several cancer types. However, mismatch repair–proficient (pMMR) metastatic colorectal cancer (CRC), ∼95% of total metastatic CRC cases, typically does not respond to ICB. Here, we show that orthotopic liver metastasis mouse models of pMMR CRC cell lines are unresponsive to ICB and recapitulate the resistance of human disease, unlike subcutaneous tumors of the same cell lines. We also show that just like the human disease, orthotopic pMMR CRC liver metastases have a paucity of T cells and dendritic cells, and that treatment with Flt3L sensitizes the liver metastases to ICB. Our findings highlight that orthotopic tumor models, and not subcutaneous models, should be used for preclinical studies of cancer immunotherapy.

IMMUNOLOGY AND INFLAMMATION

Immune checkpoint blockade (ICB) therapy has revolutionized cancer treatment in recent years. Anti–PD1 (anti–programmed cell-death protein 1) and anti–CTLA-4 (anti–cytotoxic T lymphocyte-associated protein 4) are two main types of ICB therapies that can be particularly effective (1). Metastatic melanoma, which was previously an incurable disease, now has cure rates of more than 50% when patients are treated with a combination of anti–PD1 and anti–CTLA-4 (2). However, ICB therapy is only effective in less than 15% of patients who receive the therapy (3), and efforts are ongoing to uncover the underlying mechanisms of intrinsic and acquired resistance.

Colorectal cancer (CRC) is the second leading cause of cancer-related death in the United States (4) and in the world (5). Metastatic spread, especially to the liver, is a major cause of mortality in patients with CRC (6). The efficacy of ICB therapy in metastatic CRCs has been limited to patients with mismatch repair–deficient (dMMR) or microsatellite instability-high (MSI-H) tumors, where a 55% objective response rate has been achieved (7). However, dMMR or MSI-H metastatic CRCs

Author contributions: W.W.H., I.L.G.-S., S.A., M.D., K.K., N.P.T., P.A., P.H., J.W.C., M.J.P., D.F., and R.K.J. designed research; W.W.H., I.L.G.-S., S.A., M.D., K.K., N.P.T., S.R., J.R., H.L., I.X.C., P.A., S.C., A.S.K., Z.A., Q.Z., P.H., M.R.N., V.P.C., and L.X. performed research; W.W.H., L.X., D.G.D., D.F., and R.K.J. contributed new reagents/analytic tools; W.W.H., I.L.G.-S., K.K., Z.A., M.R.N., M.J.P., and D.F. analyzed data; W.W.H., I.L.G.-S., S.A., M.D., N.P.T., J.R., H.L., P.A., S.C., A.S.K., P.H., M.R.N., V.P.C., L.X., D.G.D., J.W.C., M.J.P., D.F., and R.K.J. wrote the paper; and R.K.J. supervised research.

Reviewers: D.D., Washington University; and M.R., Oregon Health & Science University.

Competing interest statement: R.K.J. coauthored a consensus article (*Nat. Rev. Cancer* **20**, 174–186 [2020]) with one of the reviewers of this paper (D.D.). However, there was no interaction between them about anything associated with this study. R.K.J. received consultant fees from Elpis, Ophthotech, SPARC, SynDevRx, and XTuit; owns equity in Accurius, Enlight, Ophthotech, and SynDevRx; is a member of the Board of Trustees of Tekla Healthcare Investors, Tekla Life Sciences Investors, Tekla Healthcare Opportunities Fund, and Tekla World Healthcare Fund; and received a research Grant from Boehringer Ingelheim. No reagents or funding from any of these organizations was used in this study. M.J.P. has served as a consultant for Aileron Therapeutics, AstraZeneca, Cygnal Therapeutics, Elstar Therapeutics, ImmuneOncia, KSQ Therapeutics, Merck, Siamab Therapeutics, and Third Rock Ventures. These commercial relationships are unrelated to the current study. D.G.D. received consultant fees from Bayer, Simcere, Surface Oncology, and Bristol Myers Squibb, and research grants from Bayer, Exelixis, and Bristol Myers Squibb. These commercial relationships are unrelated to the current study.

[1]Present address: Singapore Immunology Network, Agency for Science, Technology and Research (A*STAR), Singapore 138648, Singapore.

[2]Present address: Department of Surgery, Tohoku University Graduate School of Medicine, Sendai 981094, Japan.

[3]Present address: Department of Breast Surgery, Kyoto University Graduate School of Medicine, Kyoto 6068507, Japan.

[4]Present address: Department of Surgery, University of Pittsburgh, Pittsburgh, PA 15213.

[5]Present address: Koch Institute for Integrative Cancer Research, Massachusetts Institute of Technology, Cambridge, MA 02139.

[6]To whom correspondence may be addressed. Email: mikael.pittet@unige.ch, dai@steele.mgh.harvard.edu, or jain@steele.mgh.harvard.edu.

This article contains supporting information online at http://www.pnas.org/lookup/suppl/doi:10.1073/pnas.2105323118/-/DCSupplemental.

Published November 1, 2021.

represent only about 5% of total metastatic CRC cases. The remaining 95% are mismatch repair–proficient (pMMR) or microsatellite stable (MSS) tumors (8), which are typically unresponsive to ICB therapy (8). Therefore, there is an urgent need to better understand the resistance mechanisms in pMMR and MSS metastatic CRCs, and improve the efficacy of treatments against this disease.

Preclinical mouse models of cancer are effective tools for studying and improving cancer therapy. MC38 and CT26 are syngeneic mouse CRC cell lines commonly used in preclinical immunocompetent mouse models of cancer. In most preclinical studies, these cells are injected under the skin into the hind flank of mice, where they grow as subcutaneous tumors. When treated with ICB therapies such as anti–PD1 and/or anti–CTLA-4, these tumors have been shown to respond well (9, 10). However, MC38 and CT26 lack coding somatic mutations in the DNA mismatch repair genes and should be considered as pMMR CRC cell lines (11, 12). Hence, experimental preclinical models using subcutaneously implanted pMMR CRC cell lines fail to recapitulate the disease resistance to ICB therapy that is observed in patients.

We hypothesized that orthotopic pMMR CRC mouse models, where pMMR CRC cells are implanted in the colon to represent primary colon tumors or in the liver to represent liver metastases, would more accurately recapitulate progression of the human disease and its response to ICB treatment in the clinic. Indeed, we report here strikingly different sensitivities to ICB treatment for pMMR CRC tumors grown orthotopically when compared with their subcutaneous counterparts. We further take advantage of these differences to define local nonmalignant components that determine the sensitivity of pMMR CRCs to treatment.

Results

CT26 and SL4 Are pMMR CRC Cell Lines with Low Tumor Mutational Burden. The mouse CRC cell lines MC38 and CT26 were previously reported to be pMMR CRC cell lines that do not carry coding somatic mutations in the DNA mismatch repair genes *Mlh1*, *Msh2*, *Msh6*, and *Pms2* (11, 12). In a separate study, MC38 was described to carry a missense mutation in the DNA mismatch repair gene *Msh3* and express a mutational signature for mismatch repair deficiency (13). To verify the mismatch repair status of MC38 and CT26, we performed whole-exome sequencing. We also sequenced the SL4 mouse CRC cell line used in our laboratory (14–16). Our analysis confirmed that MC38 lacks coding somatic mutations in *Mlh1*, *Msh2*, *Msh6*, *Pms2*, or *Mlh3* but has a missense mutation in *Msh3* (Dataset S1*A*), and therefore could potentially be dMMR. By contrast, both CT26 and SL4 lacked coding somatic mutations in *Mlh1*, *Msh2*, *Msh6*, *Pms2*, *Mlh3*, and *Msh3* (Dataset S1 *B* and *C*), and could therefore be classified as pMMR CRC cell lines (17).

The tumor mutational burden (TMB) of a patient's cancer has been shown to correlate with the objective response rate of that patient's cancer to anti–PD1 or anti–PD-L1 therapies (18). We therefore calculated the TMB of MC38, CT26, and SL4 CRC cell lines from the whole-exome sequencing data (Fig. 1*A*). Even though MC38 could be a dMMR CRC cell line, it has a TMB of 4.0 coding somatic mutations per megabase of DNA, which is comparable to human pMMR CRC (18). CT26 and SL4 also have a low TMB of 3.5 and 1.3 coding somatic mutations per megabase DNA, respectively (Fig. 1*A*). Together, these results indicate that CT26 and SL4 are functionally pMMR mouse syngeneic CRC cell lines with low TMB comparable to human pMMR CRC.

Orthotopic Liver Metastasis Mouse Models of pMMR CRC Resist ICB Therapy. Upon verifying that CT26 and SL4 are pMMR CRC cell lines, we evaluated the efficacy of anti–PD1 and anti–CTLA-4 combination treatment (here onward referred to as "ICB therapy") in subcutaneous tumor mouse models of CT26 and SL4 cells. Confirming previous reports (10, 19), we found that ICB therapy inhibited tumor growth and improved survival in both CT26 and SL4 subcutaneous tumors (Fig. 1 *B* and *C*). To determine whether the microenvironment where the cells grow had an impact on the efficacy of ICB therapy, we evaluated ICB therapy in orthotopic liver metastasis mouse models of CT26 and SL4 cells, where a hemispleen injection of cancer cells leads to the outgrowth of liver metastases (14, 20). Interestingly, we found that ICB therapy was ineffective in treating both CT26 and SL4 liver metastases, with no benefit in tumor growth or mouse survival (Fig. 1 *D* and *E*).

In the orthotopic liver metastasis mouse model we used, the hemispleen where the cancer cells are injected is removed from the mice after the injection. To eliminate the possibility that removal of the hemispleen contributed to the inefficacy of ICB therapy, we performed direct hepatic portal vein injection of CT26 and SL4 cells, in mice where the spleen is left intact (21), and treated with ICB therapy. Again, we found that both CT26 and SL4 liver metastases resisted treatment (*SI Appendix*, Fig. S1), indicating that the hemispleen removal did not cause the inefficacy of ICB therapy. We also evaluated ICB therapy in orthotopic colon tumor mouse models of CT26 and SL4 cells, where the cancer cells are injected into the cecal wall and grow into colon tumors (15, 22). We found that ICB therapy was also ineffective in treating these primary CT26 and SL4 colon tumors (Fig. 1*F* and *G*).

Altogether, these results demonstrate that the site of pMMR CRC cell growth defines the efficacy of subsequent ICB therapy. Specifically, mouse pMMR CRC cells grown in their natural microenvironments, such as the liver as liver metastases or the colon as primary tumors, better recapitulate the disease resistance to ICB therapy observed in patients.

Paucity of Activated T Cells and Dendritic Cells in ICB-Treated pMMR CRC Liver Metastases. Liver metastasis is the major cause of mortality in patients with pMMR metastatic CRC, while the primary CRC can usually be surgically removed (6). We therefore focused on the mechanisms that caused pMMR CRC liver metastases to be resistant to ICB therapy. To this end, we directly compared the microenvironments of pMMR CRC liver metastases and their subcutaneous tumor counterparts with and without ICB therapy using RNA sequencing (RNA-seq) and qPCR on bulk tumor tissues and flow cytometry (Fig. 2*A*). We found that liver metastases and subcutaneous tumors have distinct overall cell compositions and immune cell profiles (Fig. 2 *B* and *C*). $CD8^+$ T cells are the main targets of ICB therapy and kill tumor cells when ICB therapy is effective (23). We found that while the number of total $CD8^+$ T cells was not significantly different between the two sites, ICB-treated liver metastases had significantly fewer cytotoxic granzyme B+ CD8+ T cells (CT26, SL4) and activated $IFN\gamma^+TNF\alpha^+$ $CD8^+$ T cells (CT26) (Fig. 2 *D* and *E* and *SI Appendix*, Fig. S2 *A* and *B*). $CD4^+FOXP3^-$ T cells have been shown to aid the antitumor $CD8^+$ T cell response in cancer immunotherapy (24). Similar to $CD8^+$ T cells, ICB-treated SL4 and CT26 liver metastases had significantly fewer $CD4^+FOXP3^-$ T cells and activated $IFN\gamma^+TNF\alpha^+$ $CD4^+FOXP3^-$ T cells, respectively (Fig. 2 *F* and *G*). RNA-seq and gene set enrichment analysis (GSEA) confirmed that gene sets related to $CD8^+$ T cell and $CD4^+$ T cell activation were significantly down-regulated in liver metastases (Fig. 2*H*). Regulatory T (Treg) cells, which can hinder the efficacy of ICB therapy in solid tumors (25), were found in similar frequencies at both sites (*SI Appendix*, Fig. S2 *C* and *D*).

Tumor-infiltrating dendritic cells are emerging as an essential antitumor component that can foster antitumor T cell immunity and immunotherapy responses (26–29). Among these cells,

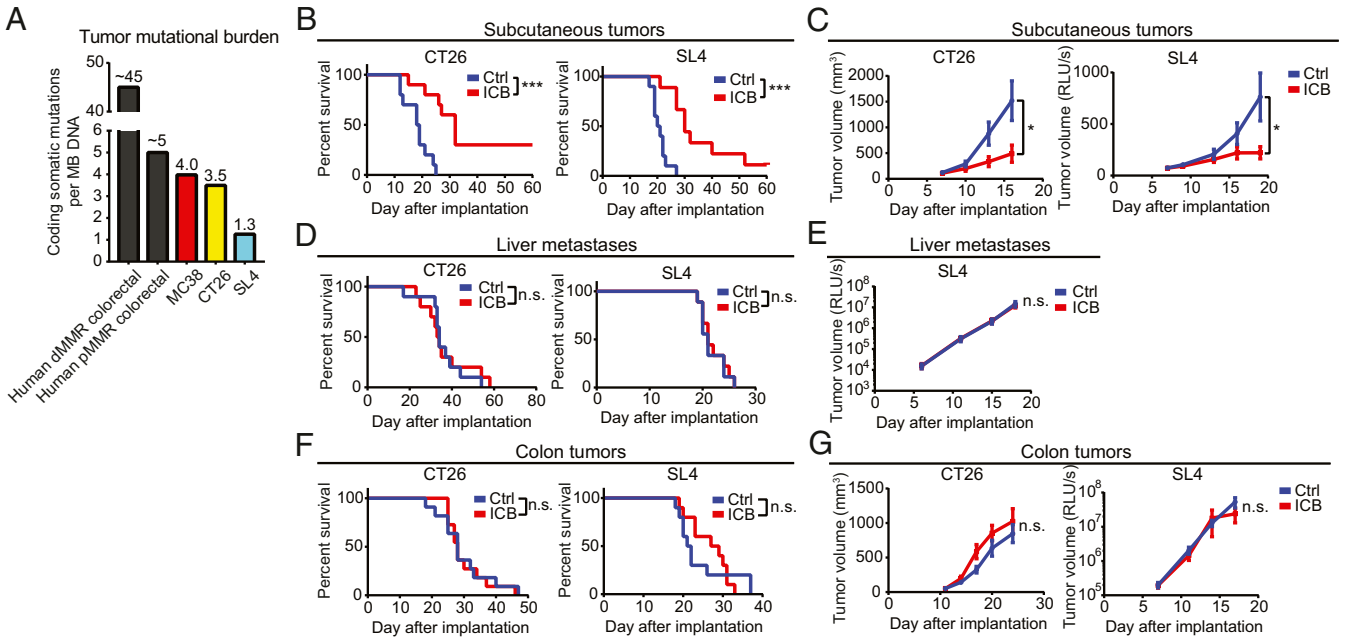

Fig. 1. Orthotopic liver metastasis mouse models of pMMR CRC recapitulate clinical inefficacy of ICB. (*A*) Number of coding somatic mutations per megabase (MB) DNA in mouse syngeneic CRC cell lines MC38, CT26, and SL4 compared with the median number in human dMMR and pMMR CRC. (*B*) Survival of mice bearing CT26 subcutaneous tumors (n = 10 per group) or SL4 subcutaneous tumors (n = 9 or 10 per group), untreated or treated with ICB therapy. ***$P < 0.001$ (log-rank test). (*C*) Tumor growth of mice bearing CT26 subcutaneous tumors (n = 10 per group) or SL4 subcutaneous tumors (n = 9 or 10 per group), untreated or treated with ICB. *$P < 0.05$ (two-tailed unpaired t test). (*D*) Survival of mice bearing CT26 liver metastases (n = 10 per group) or SL4 liver metastases (n = 10 per group), untreated or treated with ICB. n.s., not significant, $P > 0.05$ (log-rank test). (*E*) Tumor growth of mice bearing SL4 liver metastases (n = 10 per group), untreated or treated with ICB. n.s., $P > 0.05$ (two-tailed unpaired t test). There is no tumor growth curve for CT26 liver metastasis because the CT26 cell line used is not transfected with the GFP-Gluc construct. (*B–E*) Experiments were repeated at least twice and representative graphs are shown. (*F*) Survival of mice bearing CT26 colon tumors (n = 11 per group) or SL4 colon tumors (n = 10 per group), untreated or treated with ICB. n.s., $P > 0.05$ (log-rank test). (*G*) Tumor growth of mice bearing CT26 colon tumors (n = 11 per group) or SL4 colon tumors (n = 10 per group), untreated or treated with ICB. n.s., $P > 0.05$ (two-tailed unpaired t test). Data are mean ± SEM. ICB: anti–PD1 (200 μg per mouse) plus anti–CTLA-4 (100 μg per mouse); i.v. injection, three doses with a 3-d interval between doses.

those with a $CD103^+CD11b^-$ phenotype have been shown to cross-present tumor-derived antigen to $CD8^+$ T cells in subcutaneous tumor mouse models (26). We found that ICB-treated liver metastases had significantly fewer total dendritic cells, $CD103^+CD11b^-$ dendritic cells, and $CD103^-CD11b^+$ dendritic cells when compared with ICB-treated subcutaneous tumors (Fig. 3 *A* and *B*; gating strategy in *SI Appendix*, Fig. S4*A*). Using SL4 cells that express green fluorescent protein (SL4-GFP), we also found significantly fewer total dendritic cells, $CD103^+CD11b^-$ dendritic cells, and $CD103^-CD11b^+$ dendritic cells that expressed tumor-derived GFP in ICB-treated liver metastases (Fig. 3*C*). The percentage of total dendritic cells, $CD103^+CD11b^-$ dendritic cells, and $CD103^-CD11b^+$ dendritic cells that expressed tumor-derived GFP was also significantly lower in untreated liver metastases compared with untreated subcutaneous tumors (Fig. 3*D*). $CD103^+CD11b^-$ dendritic cells have been shown in subcutaneous tumor mouse models to traffic tumor antigen to tumor-draining lymph nodes (tdLNs), leading to $CD8^+$ T cell activation (30). We found that the tdLNs of ICB-treated liver metastases had significantly fewer total dendritic cells and $CD103^-CD11b^+$ dendritic cells, while $CD103^+CD11b^-$ dendritic cells showed a decreasing trend (Fig. 3*E*). Interestingly, we also found that the number of $CD103^+CD11b^-$ dendritic cells that expressed tumor-derived GFP was significantly lower in the tdLNs of ICB-treated liver metastases (Fig. 3*F*). These results indicate that there is not only poor uptake of tumor-derived antigen by dendritic cells in the liver metastases but also poor trafficking of tumor-derived antigen by dendritic cells to tdLNs to activate T cells. Gene sets related to dendritic cells were also significantly down-regulated in liver metastases (Fig. 3*G*). We did not observe a lower percentage of expression of costimulation markers such as CD80 and CD86 by dendritic cells in liver metastases (*SI Appendix*, Fig. S3*A*), which suggests that the difference in ICB response was driven primarily by the paucity of dendritic cells in the liver metastases.

Natural killer (NK) cells have been shown to recruit dendritic cells to subcutaneous tumors for effective ICB therapy (31, 32). ICB-treated liver metastases also had significantly fewer NK cells (*SI Appendix*, Fig. S3 *B* and *C*; gating strategy in *SI Appendix*, Fig. S4*B*). Gene sets related to NK cells were also significantly down-regulated in liver metastases (*SI Appendix*, Fig. S3*D*). All the gene sets that were significantly up- or down-regulated between the liver metastases and subcutaneous tumors are listed in Dataset S2.

Altogether, these results characterize the pMMR CRC liver metastasis microenvironment, which is nonresponsive to ICB therapy. In principle, this lack of response could be due to 1) the presence of molecular or cellular components that actively suppress ICB-driven antitumor immunity, 2) the absence of components required for full-fledged ICB-driven tumor control, or 3) a combination of both. To address these possibilities, we set out to dissect the mechanism(s) behind this lack of response. Table 1 and the following paragraphs summarize our findings.

Targeting Monocytes, Neutrophils, or Macrophages Does Not Sensitize pMMR CRC Liver Metastases to ICB Therapy. Potential inhibitory components to ICB efficacy include myeloid cells such as monocytes, neutrophils, and macrophages, which can promote cancer progression and limit the efficacy of treatments (33–35). For example, Ly-$6C^+$ monocytes in tumors can be immunosuppressive and limit the efficacy of anti–PD1

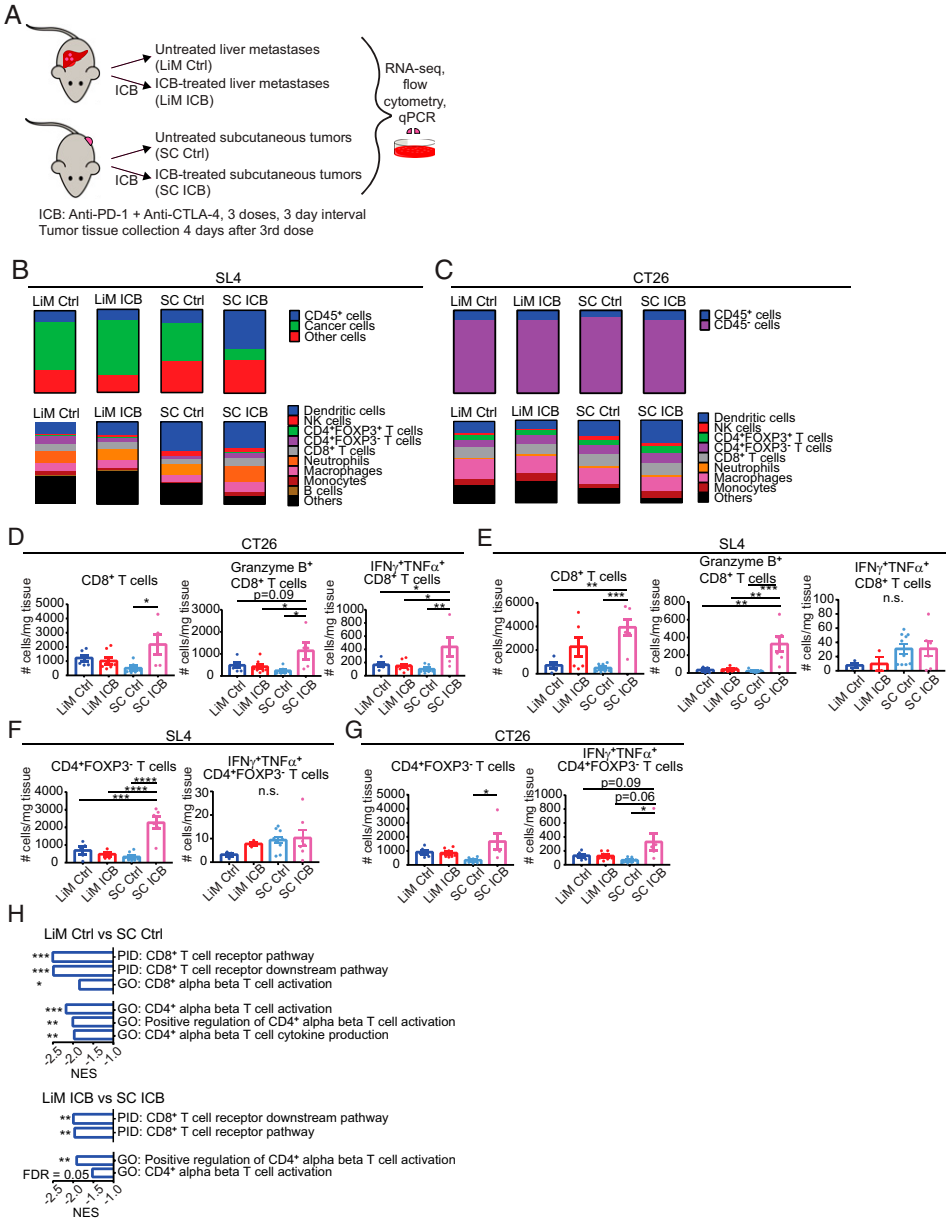

Fig. 2. pMMR CRC liver metastases have significantly fewer activated T cells than subcutaneous tumor counterparts when treated with ICB therapy. (*A*) Schematic diagram illustrating the four groups analyzed by RNA-seq, flow cytometry, and qPCR. ICB: anti–PD1 (200 μg per mouse) plus anti–CTLA-4 (100 μg per mouse), i.v. injection, three doses with a 3-d interval between doses. Tumor tissue was collected 4 d after the third dose of ICB therapy. (*B*) Average overall cell composition (n = 6 to 8 per group) and immune cell composition (n = 5 to 8 per group) of SL4 liver metastases or subcutaneous tumors, untreated or ICB-treated, determined by flow cytometry. Figure data are combined from two separate experiments. (*C*) Average overall cell composition (n = 7 to 9 per group) and immune cell composition (n = 5 to 9 per group) of CT26 liver metastases or subcutaneous tumors, untreated or ICB-treated, determined by flow cytometry. There is no cancer cell composition in the overall cell composition because the CT26 cell line used is not transfected with the GFP-Gluc construct. Figure data are combined from two separate experiments. (*D*) Number of $CD8^+$ T cells, granzyme B^+ $CD8^+$ T cells, and $IFN\gamma^+TNF\alpha^+$ $CD8^+$ T cells in CT26 liver metastases or subcutaneous tumors, untreated or ICB-treated (n = 5 to 8 per group). $^*P < 0.05$, $^{**}P < 0.01$ (one-way ANOVA with Tukey's multiple-comparisons test). (*E*) Number of $CD8^+$ T cells, granzyme B^+ $CD8^+$ T cells, and $IFN\gamma^+TNF\alpha^+$ $CD8^+$ T cells in SL4 liver metastases or subcutaneous tumors, untreated or ICB-treated (n = 3 to 10 per group). $^{**}P < 0.01$, $^{***}P < 0.001$ (one-way ANOVA with Tukey's multiple-comparisons test). Figure data are combined from two separate experiments. (*F*) Number of $CD4^+FOXP3^-$ T cells and $IFN\gamma^+TNF\alpha^+$ $CD4^+FOXP3^-$ T cells in SL4 liver metastases or subcutaneous tumors, untreated or ICB-treated (n = 3 to 10 per group). $^{***}P < 0.001$, $^{****}P < 0.0001$ (one-way ANOVA with Tukey's multiple-comparisons test). Figure data are combined from two separate experiments. (*G*) Number of $CD4^+FOXP3^-$ T cells and $IFN\gamma^+TNF\alpha^+$ $CD4^+FOXP3^-$ T cells in CT26 liver metastases or subcutaneous tumors, untreated or ICB-treated (n = 5 to 8 per group). $^*P < 0.05$ (one-way ANOVA with Tukey's multiple-comparisons test). (*H*) Significantly down-regulated $CD8^+$ T cell– or $CD4^+$ T cell–related pathways in SL4 liver metastases versus SL4 subcutaneous tumors, untreated or ICB-treated (n = 5 per group). *FDR < 0.05, **FDR < 0.01, ***FDR < 0.001 (GSEA); FDR, false discovery rate. Data are mean ± SEM. ICB treatment and tumor tissue collection schedule follows *A*. PID, Pathway Interaction Database; GO, Gene Ontology; NES, Normalized enrichment score.

treatment in glioma tumor mouse models (36), $Ly\text{-}6G^+$ neutrophils have been described with similar functions in CT26 subcutaneous tumors (10), and $CD11b^+F4/80^+$ macrophages can suppress $CD8^+$ T cells in MC38 liver metastases and prevent the efficacy of anti–PD1 or anti–PD-L1 treatment in MC38 subcutaneous tumors (37, 38). We determined that the numbers of $Ly\text{-}6C^+$ monocytes, $Ly\text{-}6G^+$ neutrophils, and $CD11b^+F4/80^+$ macrophages were not significantly increased in liver metastases compared with their subcutaneous tumor counterparts (*SI Appendix*, Fig. S5*A*; gating strategy in *SI Appendix*, Fig. S4*C*). Despite this, there is a possibility that these myeloid cell populations are more immunosuppressive in liver metastases. We therefore investigated whether depleting these myeloid cell populations could sensitize the liver metastases to ICB therapy. While anti–CSF-1 antibody treatment significantly decreased $CD11b^+F4/80^+$ macrophages and $Ly\text{-}6C^+$ monocytes in liver metastases (*SI Appendix*, Fig. S5*B*), the combination of anti–CSF-1 with ICB therapy was ineffective (*SI Appendix*, Fig. S5*C*). Similarly, anti–Gr-1 antibody treatment significantly decreased $Ly\text{-}6G^+$ neutrophils (*SI Appendix*, Fig. S5*D*), but the combination of anti–Gr-1 with ICB therapy was also ineffective (*SI Appendix*, Fig. S5*E*). These results indicate that monocytes, neutrophils, or macrophages are unlikely to play a key role in limiting the efficacy of ICB therapy in this context.

Increasing Cancer Cell MHC Class I Expression with IFN-γ Treatment Is Insufficient to Improve ICB Therapy Efficacy. Cancer cell major histocompatibility complex (MHC) class I expression is an essential component for effective immune recognition, and

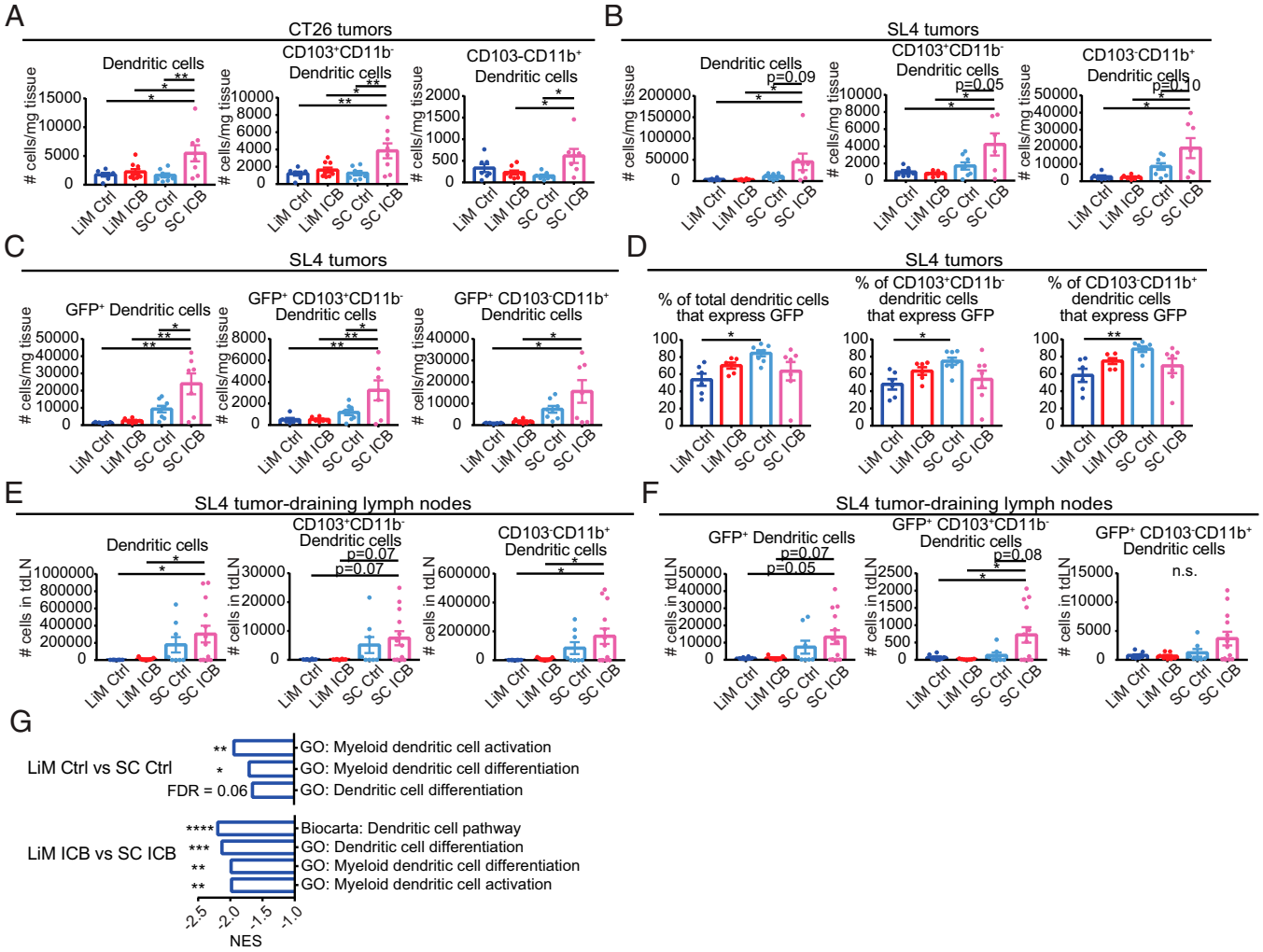

Fig. 3. pMMR CRC liver metastases have significantly fewer dendritic cells than subcutaneous tumor counterparts when treated with ICB therapy. (*A*) Number of total dendritic cells, $CD103^+CD11b^-$ dendritic cells, and $CD103^-CD11b^+$ dendritic cells in CT26 liver metastases or subcutaneous tumors, untreated or ICB-treated (n = 7 to 9 per group). *P < 0.05, **P < 0.01 (one-way ANOVA with Tukey's multiple-comparisons test). (*B*) Number of total dendritic cells, $CD103^+CD11b^-$ dendritic cells, and $CD103^-CD11b^+$ dendritic cells in SL4 liver metastases or subcutaneous tumors, untreated or ICB-treated (n = 6 to 8 per group). *P < 0.05 (one-way ANOVA with Tukey's multiple-comparisons test). (*C*) Number of total GFP^+ dendritic cells, GFP^+ $CD103^+CD11b^-$ dendritic cells, and GFP^+ $CD103^-CD11b^+$ dendritic cells in SL4-GFP liver metastases or subcutaneous tumors, untreated or ICB-treated (n = 6 to 8 per group). *P < 0.05, **P < 0.01 (one-way ANOVA with Tukey's multiple-comparisons test). (*D*) Percentages of total dendritic cells, $CD103^+CD11b^-$ dendritic cells, and $CD103^-CD11b^+$ dendritic cells that express GFP in SL4-GFP liver metastases or subcutaneous tumors, untreated or ICB-treated (n = 6 to 8 per group). *P < 0.05, **P < 0.01 (one-way ANOVA with Tukey's multiple-comparisons test). (*E*) Number of total dendritic cells, $CD103^+CD11b^-$ dendritic cells, and $CD103^-CD11b^+$ dendritic cells in tdLNs of SL4 liver metastases or subcutaneous tumors, untreated or ICB-treated (n = 6 to 8 per group). *P < 0.05 (one-way ANOVA with Tukey's multiple-comparisons test). (*F*) Number of total GFP^+ dendritic cells, GFP^+ $CD103^+CD11b^-$ dendritic cells, and GFP^+ $CD103^-CD11b^+$ dendritic cells in tdLNs of SL4-GFP liver metastases or subcutaneous tumors, untreated or ICB-treated (n = 6 to 8 per group). *P < 0.05, **P < 0.01 (one-way ANOVA with Tukey's multiple-comparisons test). (*G*) Significantly down-regulated dendritic cell–related pathways in SL4 liver metastases versus SL4 subcutaneous tumors, untreated or ICB-treated (n = 5 per group). *FDR < 0.05, **FDR < 0.01, ***FDR < 0.001, ****FDR < 0.0001 (GSEA). Data are mean ± SEM. ICB treatment and tumor tissue collection schedule follows Fig. 2*A*.

melanomas and non–small-cell lung cancers have been shown to avoid immune recognition and attack by down-regulating cancer cell MHC class I expression (39). Our GSEA showed a down-regulation of the gene set "antigen processing and presentation of endogenous antigen" in liver metastases when compared with their subcutaneous tumor counterparts (*SI Appendix*, Fig. S6*A*). In liver metastases, we also found a significantly decreased expression of genes associated with endogenous MHC class I antigen presentation (*SI Appendix*, Fig. S6*B*), and a significantly decreased MHC class I protein expression on the surface of cancer cells (*SI Appendix*, Fig. S6*C*). Interferon-gamma (IFN-γ) can increase cancer cell MHC class I expression (40) and is important for successful anti–PD1 therapy in MC38 subcutaneous tumors (28); here, we found that IFN-γ response and signaling gene sets were significantly down-regulated in liver metastases (*SI Appendix*, Fig. S6*D*). We therefore treated mice bearing liver metastases with recombinant murine IFN-γ and/or ICB therapy. IFN-γ treatment alone increased cancer cell MHC class I expression in the liver metastases to levels higher than those observed in subcutaneous tumors (*SI Appendix*, Fig. S5*C*). However, IFN-γ treatment alone did not increase tumor infiltration of total $CD8^+$ T cells or $PD1^+$ $CD8^+$ T cells (*SI Appendix*, Fig. S6*E*). The combination of IFN-γ treatment plus ICB therapy also failed to improve mouse survival (*SI Appendix*, Fig. S6 *F* and *G*). These results show that increasing cancer cell MHC class I expression with IFN-γ treatment is also insufficient to sensitize pMMR CRC liver metastases to ICB therapy.

Table 1. The effect of different interventions on the efficacy of ICB therapy in pMMR CRC liver metastases

Target	Ref.	Intervention	Effect of intervention	Efficacy of intervention as monotherapy	Efficacy of intervention in combination with ICB therapy	Fig.
Inhibitory cell type						
Ly-6C+ monocytes	(36)	Anti–CSF-1–depleting antibody	Ly-6C$^+$ monocytes significantly decreased (SL4)	Ineffective (SL4)	Ineffective (SL4)	*SI Appendix*, Fig. S5
CD11b+F4/80+ macrophages	(37, 38)	Anti–CSF-1–depleting antibody	CD11b$^+$F4/80$^+$ macrophages depleted (SL4)	Ineffective (SL4)	Ineffective (SL4)	*SI Appendix*, Fig. S5
Ly-6G+ neutrophils	(10)	Anti–Gr-1–depleting antibody	Ly-6G$^+$ neutrophils depleted (SL4)	Ineffective (SL4)	Ineffective (SL4)	*SI Appendix*, Fig. S5
Essential component/cell type						
Cancer cell MHC class I expression	(39, 40)	IFN-γ treatment	Cancer cell MHC class I expression ↑; no effect on CD8$^+$ T cells or PD1$^+$ CD8$^+$ T cells	Ineffective (SL4 and CT26)	Ineffective (SL4 and CT26)	*SI Appendix*, Fig. S6
Dendritic cells*	(41, 42)	Flt3L treatment	(Flt3L$^+$ICB) Dendritic cells, CD8$^+$ T cells, CD4$^+$FOXP3$^-$ T cells ↑ (SL4)	Ineffective (SL4); improved survival (CT26)	Flt3L+ICB better than Flt3L alone (SL4 and CT26)	Fig. 4
Dendritic cells	(43)	IFN-α treatment	Dendritic cells, CD8$^+$ T cells ↑; CD4$^+$FOXP3$^-$ T cells unchanged (SL4)	Improved survival (SL4 and CT26)	IFN-α+ICB not better than IFN-α alone (SL4 and CT26)	Fig. 5
Dendritic cells	(44, 45)	Radiation	(Radiation+ICB) Dendritic cells, CD4$^+$FOXP3$^-$ T cells, CD8$^+$ T cells ↑ (CT26) (Radiation+ICB) Dendritic cells, CD4$^+$FOXP3$^-$ T cells ↑; CD8$^+$ T cells unchanged (SL4)	Improved survival (CT26); very effective as monotherapy (SL4)	Radiation+ICB more effective than radiation alone (CT26); radiation+ICB not better than radiation alone (SL4)	Fig. 6

*Flt3L treatment in combination with ICB therapy was better than Flt3L monotherapy in both SL4 and CT26 pMMR CRC liver metastases.

Flt3L Treatment Improves Dendritic Cell Infiltration and Sensitizes pMMR CRC Liver Metastases to ICB Therapy. There is increasing evidence that dendritic cells are important in the antitumor immune response generated in effective cancer immunotherapies (27, 28). Our data also suggest that dendritic cells are likely to be insufficiently abundant in the pMMR CRC liver metastases for ICB therapy to be effective (Fig. 3 *A* and *B*). We therefore investigated strategies to improve dendritic cell infiltration in the pMMR CRC liver metastases. FMS-like tyrosine kinase 3 ligand (Flt3L) is a growth factor that promotes the expansion of dendritic cell progenitors (41, 42); we therefore treated mice bearing liver metastases with Flt3L (CDX-301; Celldex Therapeutics) and combined with ICB therapy (Fig. 4*A*). Flt3L treatment combined with ICB therapy significantly increased total dendritic cells, CD103$^+$CD11b$^-$ dendritic cells, and CD103$^-$CD11b$^+$ dendritic cells in liver metastases (Fig. 4*B*). Using SL4-GFP cells, Flt3L plus ICB therapy also increased the number of dendritic cell populations that expressed tumor-derived GFP (Fig. 4*C*). Total CD8$^+$ T cells, granzyme B$^+$ CD8$^+$ T cells, PD1$^+$ CD8$^+$ T cells, and PD1$^+$ CD4$^+$FOXP3$^-$ T cells were also significantly increased with Flt3L plus ICB therapy (Fig. 4*D* and *E*). Importantly, Flt3L plus ICB therapy significantly improved survival of mice with liver metastases and was better than Flt3L alone in both SL4 and CT26 liver metastases (Fig. 4 *F* and *G*). Altogether, these results indicate that the combination of Flt3L and ICB therapy increases intratumoral dendritic cell infiltration and T cell infiltration and activation, and is effective in treating pMMR CRC liver metastases.

IFN-α Treatment Can Improve Dendritic Cell Infiltration and Mouse Survival. Type I IFN signaling like IFN-α has been shown to be required for the accumulation of dendritic cells in tumors and antitumor T cell priming (43); type I IFN signaling and production gene sets were significantly down-regulated in liver metastases versus their subcutaneous tumor counterparts (Fig. 5*A*). We therefore determined whether treatment with recombinant murine IFN-α could increase tumor infiltration of dendritic cells in liver metastases and sensitize the tumors to ICB therapy. Indeed, IFN-α treatment alone increased the frequencies of tumor-infiltrating dendritic cells, including both CD103$^+$CD11b$^-$ and CD103$^-$CD11b$^+$ subsets, in liver metastases (Fig. 5*B*). The frequencies of CD8$^+$ T cells, including granzyme B$^+$ and PD1$^+$ subsets, also increased, whereas those of CD4$^+$FOXP3$^-$ T cells and PD1$^+$ CD4$^+$FOXP3$^-$ T cells did not (Fig. 5*C* and *D*). IFN-α treatment alone effectively improved the survival of mice with liver metastases. But, unlike Flt3L treatment, IFN-α treatment combined with ICB therapy was not better than IFN-α treatment alone in both models of pMMR CRC liver metastases (Fig. 5 *E* and *F*). These results indicate that while IFN-α treatment can improve dendritic cell infiltration and survival of mice with pMMR CRC liver metastases, it likely triggers other changes that cause the addition of ICB therapy to have no additive benefit.

Radiation plus ICB Therapy Can Improve Dendritic Cell Infiltration and Mouse Survival. Apart from directly killing cancer cells, radiation can also activate dendritic cells and increase their cross-

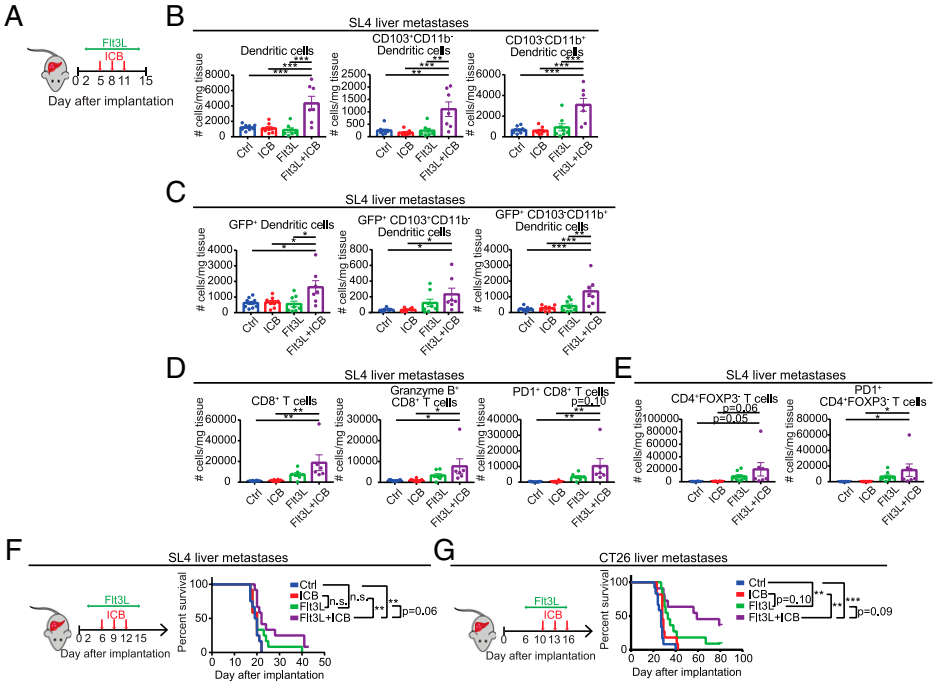

Fig. 4. Flt3L treatment improves dendritic cell infiltration and sensitizes pMMR CRC liver metastases to ICB therapy. (*A*) Schematic illustrating Flt3L treatment in mice bearing SL4 liver metastases for *B* to *E*. Flt3L is given daily, i.p., at 30 μg per mouse. (*B*) Number of total dendritic cells, $CD103^+CD11b^-$ dendritic cells, and $CD103^-CD11b^+$ dendritic cells in SL4 liver metastases, untreated or treated with ICB alone, Flt3L alone, or Flt3L plus ICB (n = 8 or 9 per group). $^{***}P < 0.001$, $^{****}P < 0.0001$ (two-tailed unpaired t test). (*C*) Number of total dendritic cells, $CD103^+CD11b^-$ dendritic cells, and $CD103^-CD11b^+$ dendritic cells that express tumor-derived GFP in SL4-GFP liver metastases, untreated or treated with ICB alone, Flt3L alone, or Flt3L plus ICB (n = 8 or 9 per group). $^{**}P < 0.01$, $^{****}P < 0.0001$ (two-tailed unpaired t test). (*D*) Number of total $CD8^+$ T cells, granzyme B^+ $CD8^+$ T cells, and $PD1^+$ $CD8^+$ T cells in SL4 liver metastases, untreated or treated with ICB alone, Flt3L alone, or Flt3L plus ICB (n = 8 or 9 per group). $^{**}P < 0.01$ (two-tailed unpaired t test). (*E*) Number of total $CD4^+FOXP3^-$ T cells and $PD1^+$ $CD4^+FOXP3^-$ T cells in SL4 liver metastases, untreated or treated with ICB alone, Flt3L alone, or Flt3L plus ICB (n = 8 or 9 per group). $^{**}P < 0.01$, $^{***}P < 0.001$ (two-tailed unpaired t test). (*F*) Survival of mice bearing SL4 liver metastases (n = 11 per group), untreated or treated with ICB alone, Flt3L alone, or Flt3L plus ICB. n.s., $P > 0.05$; $^*P < 0.01$ (log-rank test). (*G*) Survival of mice bearing CT26 liver metastases (n = 11 or 12 per group), untreated or treated with ICB alone, Flt3L alone, or Flt3L plus ICB. $^{**}P < 0.01$, $^{***}P < 0.001$ (log-rank test). Data are shown as mean ± SEM. ICB: anti–PD1 (200 μg per mouse) plus anti–CTLA-4 (100 μg/mouse); i.v. injection.

presentation of tumor antigens (44). Radiation also induces the production of type I IFN by cancer cells (45). We thus also investigated the possibility that radiation could sensitize pMMR CRC liver metastases to ICB therapy, using a conventional radiation dose of three fractions of 8 Gy (46). We found that radiation plus ICB therapy increased total dendritic cells, $CD103^+CD11b^-$ dendritic cells, and $CD103^-CD11b^+$ dendritic cells in both CT26 and SL4 liver metastases (Fig. 6 *A* and *B*). In addition, radiation plus ICB therapy increased the number of total dendritic cells, $CD103^+CD11b^-$ dendritic cells, and $CD103^-CD11b^+$ dendritic cells that expressed tumor-derived GFP in SL4-GFP liver metastases (Fig. 6*C*). Radiation plus ICB therapy also increased total $CD4^+FOXP3^-$ T cells and $PD1^+CD4^+FOXP3^-$ T cells (Fig. 6 *D* and *E*). However, radiation therapy alone and radiation plus ICB therapy only increased total $CD8^+$ T cells, granzyme B^+ $CD8^+$ T cells, and $PD1^+$ $CD8^+$ T cells in CT26 liver metastases, and not in SL4 (Fig. 6 *F* and *G*). Finally, radiation plus ICB therapy was more effective at improving mouse survival than radiation alone in CT26 liver metastases (Fig. 6*H*). By contrast, in SL4 liver metastases, radiation therapy alone was very effective, but the addition of ICB therapy did not improve survival further (Fig. 6*I*). There was no difference between the cell-intrinsic radiosensitivity of CT26 and SL4 cancer cells (*SI Appendix*, Fig. S7). These results indicate that depending on the tumor's characteristics, the combination of radiation and ICB therapy could significantly improve treatment of pMMR CRC liver metastases refractory to ICB therapy.

Human CRC Liver Metastases and MSS Primary CRC Have Fewer T Cells and Dendritic Cells than MSI-H Primary CRC and Melanomas. To further test whether our orthotopic pMMR CRC mouse models recapitulate important features of the human disease, we compared RNA-seq data of human CRC liver metastases (CRCLiM), human primary CRC (MSS) (CRCPC MSS), human primary CRC (MSI-H) (CRCPC MSI-H), and human melanomas (SKCM); all of these tumors had received no prior treatment. We considered these different tumor types because our orthotopic liver metastasis and colon tumor models represent CRC liver metastases and MSS primary CRC, respectively, while MSI-H CRC and melanomas are two of the most responsive tumor types to ICB therapy (2, 7). From the RNA-seq data, we calculated the gene set variation analysis (GSVA) enrichment scores for different immune cell types with previously published gene expression profiles (47). We found that human CRC liver metastases and MSS primary CRCs had significantly lower enrichment scores for activated $CD4^+$ T cells than MSI-H primary CRCs (Fig. 7*A*). CRC liver metastases and MSS primary CRCs also had significantly lower enrichment scores for central memory $CD4^+$ T cells, central memory $CD8^+$ T cells, and effector memory $CD8^+$ T cells than MSI-H primary CRCs and melanomas (Fig. 7 *A* and *B*). In addition, enrichment scores for activated and immature dendritic cells were also lower in CRC liver metastases and MSS primary CRCs (Fig. 7*C*). These human data suggest that, similar to our orthotopic mouse models, human CRC liver metastases and MSS primary CRC have a paucity of T cells and dendritic cells.

Discussion

The tumor microenvironment where cancer cells are grown in preclinical mouse models has been shown to significantly affect the resultant tumors' growth and response to therapies (48–52). For CRC, there have been several studies showing that anti–PD1 and/or anti–CTLA-4 ICB treatments are very effective in treating subcutaneous tumor models of MC38 or CT26 CRC grown in syngeneic mice (9, 10, 19). However, the comparison of the efficacy of ICB therapy in orthotopic CRC liver metastasis mouse models in immunocompetent mice with subcutaneous tumor models has not been studied in great detail.

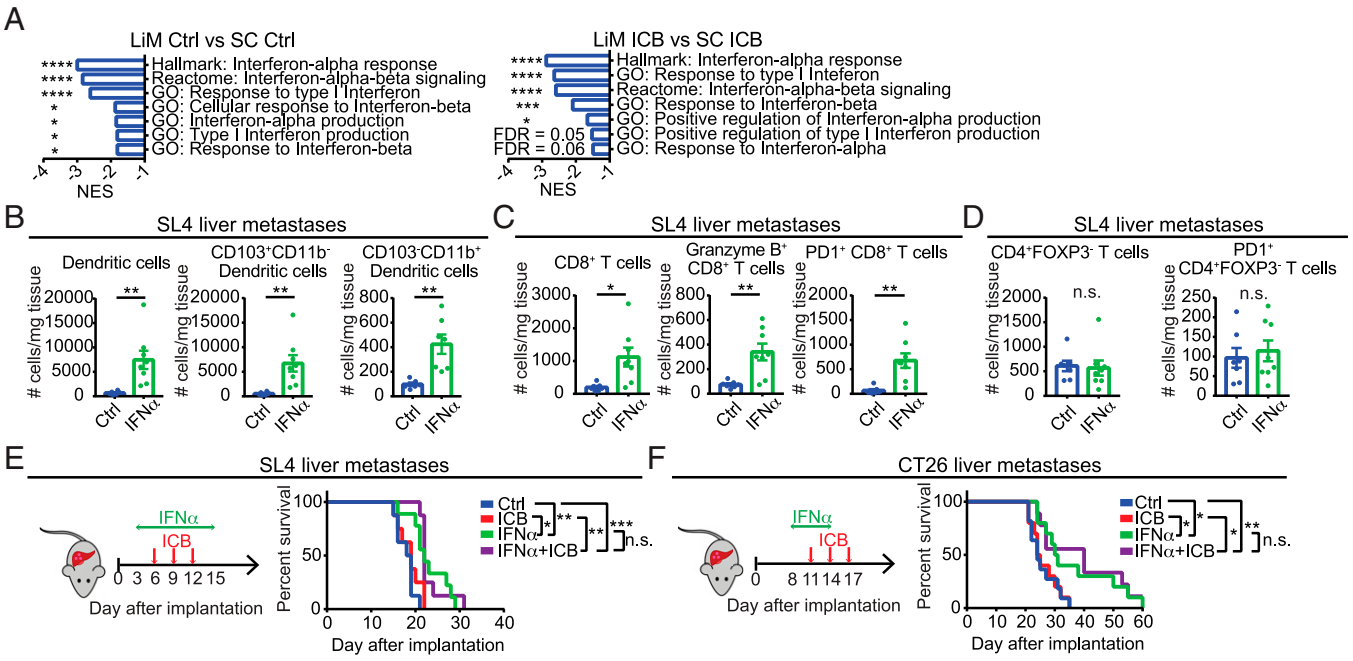

Fig. 5. IFN-α treatment can improve dendritic cell infiltration and mouse survival. (*A*) Significantly down-regulated type I IFN-related pathways in SL4 liver metastases versus SL4 subcutaneous tumors, untreated or ICB-treated ($n = 5$ per group). *FDR < 0.05, **FDR < 0.01, ****FDR < 0.0001 (GSEA). (*B*) Number of total dendritic cells, $CD103^+CD11b^-$ dendritic cells, and $CD103^-CD11b^+$ dendritic cells in SL4 liver metastases, untreated or treated with IFN-α ($n = 7$ or 8 per group). **$P < 0.01$ (two-tailed unpaired t test). (*C*) Number of total $CD8^+$ T cells, granzyme B^+ $CD8^+$ T cells, and $PD1^+$ $CD8^+$ T cells in SL4 liver metastases, untreated or treated with IFN-α ($n = 7$ or 8 per group). *$P < 0.05$, **$P < 0.01$ (two-tailed unpaired t test). (*D*) Number of total $CD4^+FOXP3^-$ T cells and $PD1^+$ $CD4^+FOXP3^-$ T cells in SL4 liver metastases, untreated or treated with IFN-α ($n = 7$ or 8 per group). n.s., $P > 0.05$ (two-tailed unpaired t test). (*B–D*) IFN-α: 20,000 units daily, i.p., 11 d. Tumor tissue collection: day after last treatment. (*E*) Survival of mice bearing SL4 liver metastases ($n = 8$ or 9 per group), untreated or treated with ICB alone, IFN-α alone, or IFN-α plus ICB. n.s., $P > 0.05$; *$P < 0.05$, **$P < 0.01$, ***$P < 0.001$ (log-rank test). IFN-α: 20,000 units daily, i.p., on the indicated days. (*F*) Survival of mice bearing CT26 liver metastases ($n = 8$ to 11 per group), untreated or treated with ICB alone, IFN-α alone, or IFN-α plus ICB. n.s., $P > 0.05$; *$P < 0.05$, **$P < 0.01$ (log-rank test). IFN-α: 20,000 units daily, i.p., on the indicated days. Data are mean ± SEM. ICB: anti–PD-1 (200 μg per mouse) plus anti–CTLA-4 (100 μg per mouse); i.v. injection.

We characterized three different mouse CRC cell lines, MC38, CT26, and SL4, and determined that CT26 and SL4 are pMMR CRC cell lines with low TMB. We then show that anti–PD1 plus anti–CTLA-4 (ICB therapy) is ineffective in treating CT26 and SL4 orthotopic liver metastases in mice, which recapitulates the clinical experience with pMMR metastatic CRC patients. On the contrary, we show that ICB therapy is very effective in treating subcutaneous tumors of the same cell lines. Also, many studies have used subcutaneous tumors assuming that these models represent the characteristics of primary tumors, for example subcutaneously grown prostate cancer to represent primary prostate cancers (51) and subcutaneously grown MC38 tumors to represent primary colon tumors (37). We show that when CT26 and SL4 are grown in the colon as primary colon tumors, ICB therapy is ineffective in treating the resultant colon tumors, a significant contrast compared with its strong efficacy in treating their subcutaneous tumor counterparts. Our results emphasize that the microenvironment where cancer cells grow can significantly influence their response to therapy, especially immunotherapy such as ICB, and that to best recapitulate in preclinical studies what is observed in human patients, cancer cells should be grown in the appropriate anatomical location of the mouse. In the case of pMMR CRC cell lines like CT26 and SL4, these should be grown either in the liver as liver metastases or in the colon as primary colon tumors. Our results also corroborate the known tolerogenic properties of the liver microenvironment which has been shown to influence antigen-presenting cell function (53) and adaptive immunity (54). In addition, widely used subcutaneous tumor models appear to be overly sensitive to immunotherapy approaches. Therefore, caution should be exercised in interpreting and translating such results.

Our study is a cautionary tale that in order for preclinical mouse studies to better predict or recapitulate the response of human cancer patients to different treatments, the correct orthotopic mouse models have to be used. We refer to a preclinical study that showed that the combination of MEK inhibition and anti–PD-L1 therapy had durable responses in CT26 subcutaneous tumors (55). This preclinical study eventually led to a phase III clinical trial that evaluated the combination of the MEK inhibitor cobimetinib and the anti–PD-L1 therapy atezolizumab in metastatic CRC patients, with a majority of patients enrolled having pMMR tumors. Unfortunately, the phase III clinical trial failed to meet the desired primary end point of overall survival (56). Although we do not prove definitively that using an orthotopic tumor model might have helped reach a clinically relevant conclusion for this drug combination, we show that mouse models of orthotopic pMMR CRC liver metastasis can more accurately recapitulate ineffective ICB therapy in patients with pMMR metastatic CRC. These orthotopic liver metastasis mouse models should also be useful tools for the preclinical evaluation of novel drug combinations for patients with pMMR CRC liver metastasis, especially combinations involving ICB therapy (57).

Dendritic cells have a vital role in cancer immunity and immunotherapy (29), and we found a clear paucity of dendritic cells in the ICB-treated pMMR CRC liver metastases. The administration of Flt3L, a growth factor involved in the expansion of dendritic cell progenitors (58), has been shown to improve cancer immunosurveillance in mice (42) and to increase response to anti–PD-L1 therapy in mouse melanoma lesions (41). Here, we show that Flt3L treatment plus ICB therapy can increase the infiltration of dendritic cells, $CD4^+$

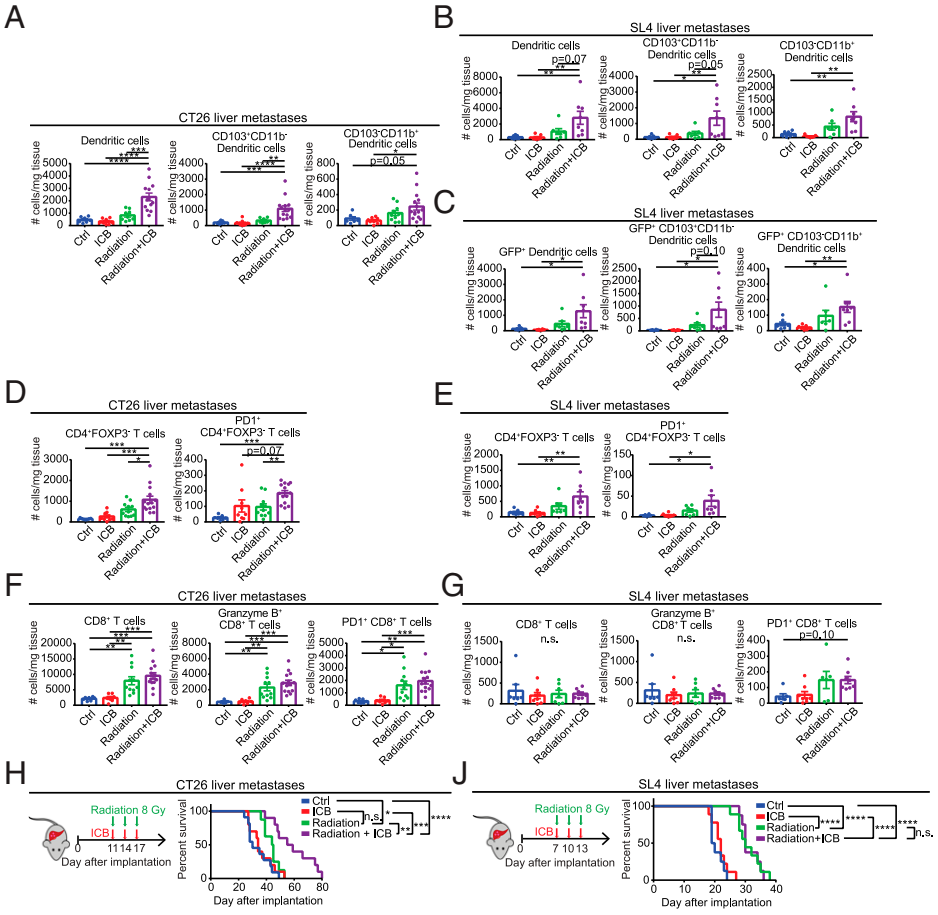

Fig. 6. Radiation plus ICB therapy can improve dendritic cell infiltration and mouse survival. (*A*) Number of total dendritic cells, $CD103^+CD11b^-$ dendritic cells, and CD103−CD11b+ dendritic cells in CT26 liver metastases, untreated or treated with ICB alone, radiation alone, or radiation plus ICB (n = 7 to 15 per group). *P < 0.05, **P < 0.01, ***P < 0.001, ****P < 0.0001 (one-way ANOVA with Tukey's multiple-comparisons test). There is no GFP^+ dendritic cell data for CT26 liver metastasis because the CT26 cell line used is not transfected with the GFP-Gluc construct. (*B*) Number of total dendritic cells, $CD103^+CD11b^-$ dendritic cells, and $CD103^-CD11b^+$ dendritic cells in SL4 liver metastases, untreated or treated with ICB alone, radiation alone, or radiation plus ICB (n = 7 or 8 per group). *P < 0.05, **P < 0.01 (one-way ANOVA with Tukey's multiple-comparisons test). (*C*) Number of total dendritic cells, $CD103^+CD11b^-$ dendritic cells, and $CD103^-CD11b^+$ dendritic cells that express tumor-derived GFP in SL4-GFP liver metastases, untreated or treated with ICB alone, radiation alone, or radiation plus ICB (n = 7 or 8 per group). *P < 0.05, **P < 0.01 (one-way ANOVA with Tukey's multiple-comparisons test). (*D*) Number of total $CD4^+FOXP3^-$ T cells and $PD1^+$ $CD4^+FOXP3^-$ T cells in CT26 liver metastases, untreated or treated with ICB alone, radiation alone, or radiation plus ICB (n = 7 to 15 per group). *P < 0.05, **P < 0.01, ***P < 0.001 (one-way ANOVA with Tukey's multiple-comparisons test). (*E*) Number of total $CD4^+FOXP3^-$ T cells and $PD1^+$ $CD4^+FOXP3^-$ T cells in SL4 liver metastases, untreated or treated with ICB alone, radiation alone, or radiation plus ICB (n = 7 or 8 per group). *P < 0.05, **P < 0.01 (one-way ANOVA with Tukey's multiple-comparisons test). (*F*) Number of total $CD8^+$ T cells, granzyme B^+ $CD8^+$ T cells, and $PD1^+$ $CD8^+$ T cells in CT26 liver metastases, untreated or treated with ICB alone, radiation alone, or radiation plus ICB (n = 7 to 15 per group). *P < 0.05, **P < 0.01, ***P < 0.001 (one-way ANOVA with Tukey's multiple-comparisons test). (*G*) Number of total $CD8^+$ T cells, granzyme B^+ $CD8^+$ T cells, and $PD1^+$ $CD8^+$ T cells in SL4 liver metastases, untreated or treated with ICB alone, radiation alone, or radiation plus ICB (n = 7 or 8 per group). n.s., P > 0.05 (one-way ANOVA with Tukey's multiple-comparisons test). (*A*, *D*, and *F*) Radiation: 8 Gy; ICB: days 11, 14, and 17; tumor tissue collection: day 20. (*B*, *C*, *E*, and *G*) Radiation: 8 Gy; ICB: days 7, 10, and 13; tumor tissue collection: day 17. (*H*) Survival of mice bearing CT26 liver metastases (n = 8 to 11 per group), untreated or treated with ICB alone, radiation alone, or radiation plus ICB. n.s., P > 0.05; *P < 0.05, **P < 0.01, ***P < 0.001, ****P < 0.0001 (log-rank test). (*I*) Survival of mice bearing SL4 liver metastases (n = 8 or 9 per group), untreated or treated with ICB alone, radiation alone, or radiation plus ICB. n.s., P > 0.05; ****P < 0.0001 (log-rank test). Data are mean ± SEM. ICB: anti–PD1 (200 μg per mouse) plus anti–CTLA-4 (100 μg per mouse); i.v. injection.

$FOXP3^-$ T cells, and $CD8^+$ T cells in pMMR CRC liver metastases that were previously lacking in these immune cell types. We also show that Flt3L treatment plus ICB therapy significantly improved mouse survival and was better than Flt3L treatment alone in two models of pMMR CRC liver metastases. These results indicate that the combination of Flt3L plus ICB therapy could potentially be an effective treatment option for patients with pMMR CRC liver metastases, a tumor type that has typically very poor response to immunotherapy, and warrants further investigation.

We also used IFN-α treatment to improve dendritic cell infiltration in the liver metastases and determined subsequent ICB efficacy. While IFN-α treatment successfully increased dendritic cell infiltration and $CD8^+$ T cell activation and improved mouse survival as a monotherapy, the addition of ICB therapy to IFN-α treatment had no additional benefit. Possible explanations for this include the lack of increase in $CD4^+FOXP3^-$ T cells, or that IFN signaling in cancer cells can up-regulate a tumor-intrinsic resistance program against ICB treatment (59). Prolonged IFN treatment can also cause terminal exhaustion of the $CD8^+$ T cells (40). Therefore, more work has to be performed to understand the interaction of IFN-α treatment and ICB therapy in the treatment of pMMR CRC liver metastases (60). Radiation can also activate dendritic cells in tumors (44), and has been shown to synergize with various ICB therapies in subcutaneous tumors (61, 62). We found that whole-liver irradiation plus ICB therapy successfully increased dendritic cell and $CD4^+FOXP3^-$ T cell infiltration into both models of pMMR CRC liver metastases. But only in CT26, the model with higher TMB, was radiation plus ICB therapy more effective than radiation alone. These results raise the important clinical question regarding which pMMR metastatic CRC patients would likely benefit from a combination of radiation plus ICB, and which patients would be able to achieve a durable response with radiation alone (46, 63). Our data suggest that patients with a higher TMB might be more likely to benefit from a combination of radiation plus ICB. A deeper understanding of the differences in mechanisms involved in these two models is necessary toward selecting the best treatment for patients with pMMR metastatic CRC.

In conclusion, we strongly recommend that orthotopic tumor models, and not subcutaneous tumor models, be used to inform the design of human clinical trials, especially in pMMR metastatic CRC. We also show that ICB therapy resistance in

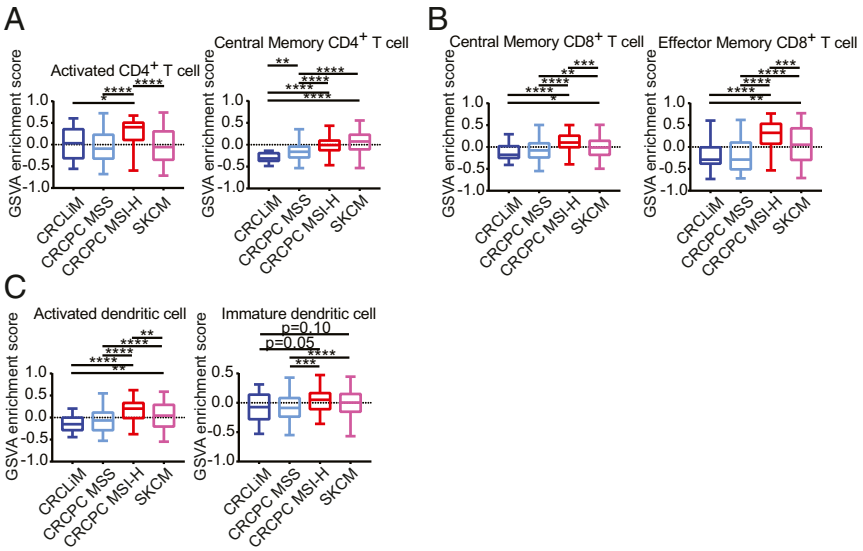

Fig. 7. Human CRC liver metastases and MSS CRC primary tumors have a paucity of $CD4^+$ T cells, $CD8^+$ T cells, and dendritic cells. (*A*) GSVA enrichment score of activated $CD4^+$ T cells and central memory $CD4^+$ T cells in human CRC liver metastases (CRCLiM), MSS CRC primary tumors (CRCPC MSS), MSI-H CRC primary tumors (CRCPC MSI-H), and melanoma tumors (SKCM). $*P < 0.05$, $**P < 0.01$, $****P < 0.0001$ (one-way ANOVA with Tukey's multiple-comparisons test). (*B*) GSVA enrichment score of central memory $CD8^+$ T cells and effector memory $CD8^+$ T cells in human CRC liver metastases (CRCLiM), MSS CRC primary tumors (CRCPC MSS), MSI-H CRC primary tumors (CRCPC MSI-H), and melanoma tumors (SKCM). $*P < 0.05$, $**P < 0.01$, $***P < 0.001$, $****P < 0.0001$ (one-way ANOVA with Tukey's multiple-comparisons test). (*C*) GSVA enrichment score of activated dendritic cells and immature dendritic cells in human CRC liver metastases (CRCLiM), MSS CRC primary tumors (CRCPC MSS), MSI-H CRC primary tumors (CRCPC MSI-H), and melanoma tumors (SKCM). $*P < 0.05$, $**P < 0.01$, $***P < 0.001$, $****P < 0.0001$ (one-way ANOVA with Tukey's multiple-comparisons test). CRCLiM: $n = 25$; CRCPC MSS: $n = 336$; CRCPC MSI-H: $n = 58$; SKCM: $n = 473$. Data are mean ± SEM.

pMMR CRC liver metastases can be mitigated by increasing the frequency of dendritic cells to promote infiltration and activation of effector T cells.

Methods

Mice. Male 6- to 10-wk-old C57BL/6 wild-type (WT) and BALB/c WT mice were used in the animal experiments. Mice were bred and maintained in the Edwin L. Steele gnotobiotic animal facility at Massachusetts General Hospital (MGH). All mouse experiments strictly abided by the Public Health Service Policy on Humane Care of Laboratory Animals. All mouse experimental procedures performed were approved by the Institutional Animal Care and Use Committee at MGH.

Cell Lines. The CT26 mouse CRC cells were purchased from the American Type Culture Collection. The SL4 mouse CRC cells were a kind gift from T. Irimura (Graduate School of Pharmaceutical Sciences, Tokyo University, Tokyo, Japan) (16). The MC38 mouse CRC cells were a kind gift from A. Sharpe (Department of Immunology, Harvard Medical School, Boston, MA). SL4 cells were cultured in Dulbecco's modified Eagle's medium/F12 (1:1) supplemented with 10% fetal bovine serum (FBS). CT26 and MC38 were cultured in RPMI-1640 medium supplemented with 10% FBS. For in vivo implantation, the cells were grown to ~70% confluency, washed with phosphate-buffered saline (PBS), counted, and resuspended in the appropriate media. SL4 cells transfected previously with a lentiviral vector encoding both GFP and Gluc (14) were also used.

Mouse Tumor Models. The orthotopic liver metastasis mouse model that we used throughout the manuscript is a hemispleen injection model that has been described previously (14). Briefly, the spleen was split into two sectors, and 50,000 cancer cells were injected into the distal caudal sector, which was then resected. The other sector of the spleen was kept in place to maintain systemic immunity. CT26 tumor formation in the liver was confirmed by a high-frequency ultrasound imaging system (VisualSonic Vevo 2100 System) and SL4 tumor burden was measured by blood *Gaussia* luciferase (Gluc) secreted from Gluc-transduced tumors (64, 65). Direct hepatic portal vein injection was also used for the orthotopic liver metastasis mouse model only when stated in the text (21).

The orthotopic primary colon tumor mouse model we used has also been described previously (15). Briefly, the cecum was exteriorized, and 500,000 cancer cells were injected into the cecal wall between the serosa and mucosa from the serosal side. Tumor burden was monitored similarly by either ultrasound or blood Gluc measurements.

For the subcutaneous tumor mouse models, 500,000 cancer cells were injected under the skin of the hind flank of the mice. Calipers were used to measure tumor volume and monitor tumor growth.

In all models, mouse death was determined when the tumor volume exceeds 1,600 mm^3 or when the mouse reaches a moribund state.

Drug Treatments. For all in vivo studies, mice were randomized by tumor volume measured by ultrasound or calipers, or by blood Gluc concentration.

For ICB treatment, 200 μg of anti–PD1 from BioXCell (clone RMP1-14) and 100 μg of anti–CTLA-4 from BioXCell (clone 9D9) were given intravenously (i.v.) every 3 d for a total of three doses. For the SL4 liver metastasis mouse model, ICB treatment was started when blood Gluc values had increased significantly from baseline values of $\sim 1 \times 10^3$ relative light units per second (RLU/s) to values greater than 3×10^3 RLU/s. For the CT26 liver metastasis mouse model, ICB treatment was started when metastasis was visible by ultrasound (when metastatic nodules were $\sim 1 \times 1$ mm). For the CT26 primary colon tumor mouse model, ICB was started when the average tumor size was about 4×4 mm by ultrasound. For SL4 and CT26 subcutaneous tumor mouse models, ICB was started on day 7 post tumor implantation when the average tumor size was about 4×4 mm.

Anti-mouse Gr-1 from BioXCell (clone RB6-8C5) (250 μg) was given intraperitoneally (i.p.) every 3 d starting 1 to 2 d before the first ICB treatment. Anti-mouse CSF-1 from BioXCell (clone 5A1) was given i.p. every 4 d starting 1 to 2 d before the first ICB treatment. The first anti-mouse CSF-1 dose was 1 mg per mouse, with subsequent doses being 0.5 mg per mouse. Five thousand or 10,000 units of murine recombinant IFN-γ from PeproTech (315-05) was given i.v. daily for the stated duration. Twenty thousand units of murine recombinant IFN-α from BioLegend (752808) was given i.p. daily (66) for the stated duration. Thirty micrograms of Flt3L (CDX-301) from Celldex Therapeutics was given i.p. daily (41, 42) for the stated duration.

Radiation Therapy. Irradiation of mice was performed using an X-RAD 320 Irradiation System (Precision X-Ray), one mouse at a time. The mouse first had hair removed from its abdomen using hair removal cream. Ultrasound imaging (VisualSonic Vevo 2100 System) was then used to locate the liver of the mouse. The mouse was then secured to a mouse holder and a lead block with a hole of diameter 20 mm was placed on top of the abdomen of the mouse, with the hole exposing the part of the mouse to be irradiated. The whole liver of the mouse was then irradiated with a vertical X-ray beam at a dose rate of 3.5 Gy/min. Mice were irradiated with three doses of 8-Gy radiation, with a 3-d interval between doses, concomitant with ICB therapy.

Whole-Exome Sequencing of Mouse Syngeneic Cancer Cell Lines. Whole-exome sequencing was performed by the Beijing Genomics Institute. Genomic DNA (1 μg) was first randomly fragmented by Covaris. Fragmented DNA was selected by an Agencourt AMPure XP-Medium Kit to an average size of 200 to 400 bp. The selected fragments were end-repaired, 3′-adenylated, adapter-ligated, and PCR-amplified and the products were recovered using the AxyPrep Mag PCR Clean-Up Kit. The PCR products were hybridized with Agilent Hybridization and Wash Kits. After that, the AxyPrep Mag PCR Clean-Up Kit was used to recover the products as before. The double-stranded PCR products were heat-denatured and circularized by the splint oligo sequence, forming the final library of single-stranded circular DNA. The library was amplified to make DNA nanoballs (DNBs). The DNBs were loaded into the patterned nanoarray and paired-end 100 base reads were generated by sequencing with combinatorial probe–anchor synthesis on the DNBseq platform.

Analysis of Whole-Exome Sequencing Data. Raw FASTQ files were trimmed using Trimmomatic (67). Trimmed FASTQ files were aligned to the mouse Ensembl GRCm38 reference genome using the Burrows–Wheeler Aligner (68), MEM algorithm. The Genome Analysis Toolkit (69) was used to call variants between the cancer cell line and the reference genome. For CT26, germline variants present in the Balb/c mouse strain were subtracted from the called variants. Functional impact of single-nucleotide polymorphisms (SNPs) and indels was annotated using SnpEff (70).

Flow Cytometry. Liver metastasis nodules were isolated from normal liver tissue in mice bearing liver metastasis. Subcutaneous tumors were excised from the mouse's flank. The isolated tumors were diced into small pieces and incubated in digestion buffer (1.5 mg/mL collagenase, 1.5 mg/mL hyaluronidase, and 20 μg/mL DNase in Hanks' balanced salt solution) for 1 h. The resulting suspension was passed through 70-μm cell strainers and centrifuged. The supernatant was discarded, and the cell pellet was resuspended in ammonium-chloride-potassium lysing buffer to lyse the red blood cells. The resulting suspension was centrifuged, resuspended in flow cytometry staining buffer (2% FBS in PBS), and passed through 40-μm cell strainers. The resulting single-cell suspension was then split into aliquots for appropriate staining of flow cytometry antibodies.

For tdLN analysis of liver metastases, the portal, celiac, and first mesenteric LNs that drain the liver were collected (71). For tdLN analysis of subcutaneous tumors, the inguinal LNs on the same flank as the subcutaneous tumor were collected. The collected tdLNs were meshed through 70-μm cell strainers, centrifuged, resuspended in flow cytometry staining buffer, passed through 40-μm cell strainers, and split into aliquots for staining.

For blocking of Fc receptors, the anti-mouse CD16/32 antibody (clone 93) was used. Antibodies were purchased from BioLegend unless specified otherwise. For extracellular staining, the following antibodies were used: CD45-PerCP, CD45-Alexa700 (clone 30-F11), CD3-PE-Dazzle (clone 17A2), CD4-PE-Cy7 (clone RM4-5), CD8-APC-Cy7 (clone 53-6.7), NK1.1-PE (clone PK136), PD-1-PE (clone 29F.1A12), CD11c-FITC, CD11c-BV605 (clone N418), F4/80-APC-Cy7 (clone BM8), Ly-6C-APC (clone HK1.4), MHCII-PE (clone M5/114.15.2), CD24-Alexa700 (clone M1/69), CD11b-PE-Dazzle (clone M1/70), B220-APC-Cy7 (clone RA3-6B2), NKp46-APC (clone 29A1.4), CD49b-PE-Cy7 (clone DX5), CD103-PE-Cy7 (clone 2E7), CD80-BV421 (clone 16-10A1), CD86-BV510 (clone GL-1), MHCI-Alexa647 (clone 28-8-6), MHCI-APC (clone 34-1-2S), Ly-6G-PE (clone 1A8), and CD206-Alexa700 (clone C068C2). For intracellular staining, the eBioscience Foxp3/transcription factor staining buffer set and the following antibodies were used: granzyme B-FITC (clone GB11), FOXP3-APC (clone FJK-16s; eBioscience), IFN-γ-Alexa700 (clone XMG1.2), and TNFα-PE (clone MP6-XT22). For intracellular staining of cytokines, cells were incubated for 4 h in the cell activation mixture (with brefeldin A) from BioLegend.

The stained single-cell suspensions were recorded on either a BD LSR II or a BD Fortessa X-20 flow cytometry machine. The FCS data files were then analyzed by FlowJo v10.

RNA Extraction and qRT-PCR. Tumor samples were snap-frozen in liquid nitrogen and stored at −80 °C. RNA was extracted from the frozen tumor samples using the QIAGEN RNeasy Mini Kit. Complementary DNA was synthesized from extracted RNA using iScript Reverse Transcription Supermix (Bio-Rad Laboratories). Relative gene expressions of various genes were determined using SYBR Green PCR Master Mix (Applied Biosystems), their respective forward and reverse primers, and a Stratagene Mx3000P qPCR System. All gene expression values were normalized to the expression of mouse glyceraldehyde-3-phosphate dehydrogenase (GAPDH).

RNA-seq. Sequencing of extracted RNA from bulk tumor tissue was performed by the Massachusetts Institute of Technology BioMicro Center. A Fragment Analyzer (Advanced Analytical Technologies) was used to confirm the quality of the RNA samples. The Kapa HyperPrep Kit (Roche) was then used to prepare and index Illumina libraries from ∼250 ng of total RNA. The libraries were confirmed using the Fragment Analyzer, and qPCR was used to quantify the libraries. The libraries were then pooled and sequenced on an Illumina NextSeq 500 with 40 + 40 paired-end reads. Custom scripts were used to demultiplex the samples and allow single mismatches to the index sequencing.

Analysis of RNA-seq Data. STAR (72) was used to align the raw FASTQ files to the mouse Ensembl GRCm38 reference genome. Gene read counts were then generated using the Bioconductor R package GenomicAlignments (73). Differentially expressed genes and normalized gene read counts were obtained using DESeq2 (74). GSEA software from the Broad Institute (75, 76) was used to perform GSEA.

Analysis of Publicly Available Human Datasets. Raw RNA-seq counts of human CRC liver metastases with no prior treatment were downloaded from GSE145432 (77) and GSE151165 (78). Raw RNA-seq counts of human primary CRC (both MSS and MSI-H) and melanomas, all untreated, were downloaded from The Cancer Genome Atlas (TCGA). Gene expression profiles for different immune cell types were obtained from Charoentong et al. (47). GSVA (79) was used to obtain GSVA enrichment scores for each immune cell type.

Radiosensitivity Measurements. Single-cell suspensions were prepared, counted, and seeded (1.0×10^5 cells) into 25-cm^2 flasks 20 to 24 h before experiments. Then, cells were trypsinized, divided, and plated (50 to 2,500 cells) into each well of the 6-well plates, and irradiated 3 h later with a 320-kV, 12.5-mA X-ray at a nominal dose rate of 1.67 Gy/min (five doses: 0 to 8 Gy in 2-Gy increments). Cells were then incubated for 7 to 10 d for colony formation following the irradiation exposure depending on the dose administered. The surviving fraction data were corrected for initial and final multiplicity (80). The in vitro experiments were repeated at least three times.

Statistical Analyses. Statistical analyses were all performed in GraphPad Prism 7.

Data Availability. Raw RNA-sequencing data of mouse liver metastases and subcutaneous tumors performed in this study have been deposited in the National Center for Biotechnology Information (NCBI) Sequence Read Archive under BioProject ID code PRJNA710489. All study data are included in the article and/or supporting information.

ACKNOWLEDGMENTS. We thank Takashi Nojiri and Julia Kahn for help with tumor implantation and tissue collection, Yuhui Zhao for help with tissue collection, and Mark Duquette and Carolyn Smith for technical support. We also thank Paula Hammond and Robert Langer for useful advice. The human data shown in this manuscript are in part based upon data generated by the TCGA Research Network (https://www.cancer.gov/about-nci/organization/ccg/research/structural-genomics/tcga). R.K.J. was supported in part by NIH Grants P01-CA080124, R35-CA197743, U01-CA224348, R01-CA208205, and R01-CA259253, the Harvard Ludwig Cancer Center Advanced Medical Research Foundation, and Jane's Trust Foundation. D.F. was supported in part by NIH Grants P01-CA080124, R01-CA208205, and R01-NS118929. M.J.P. was supported in part by NIH Grants R01-AI084880, R01-CA218579, R01-CA206890, and U01-CA224348 and the Institut Suisse de Recherche Experimentale sur le Cancer (ISREC, Swiss Institute for Experimental Cancer Research) Foundation. D.G.D. was supported in part by Department of Defense Awards W81XWH-19-1-0284 and W81XWH-19-1-0482 and NIH Grants P01-CA080124, R01-CA260872, and R01-CA260857. W.W.H. and A.S.K. were supported in part by Agency for Science, Technology and Research (A*STAR) Graduate Scholarships. N.P.T. was supported by Cancer Research Institute's (CRI) Irvington/Merck Fellowship. J.R. was a CRI-Dr. Keith Landesman Memorial Fellow and supported in part by CRI Irvington Postdoctoral Fellowship and Fund for Medical Discovery Fellowship from Massachusetts General Hospital. S.C. was supported in part by Jane's Trust Foundation, an American Brain Tumor Association Basic Research Fellowship, and the Pediatric Cancer Research Foundation. The RNA-sequencing work in this study was partially funded by National Cancer Institute Koch Institute Support (core) Grant P30-CA14051.

1. A. Ribas, J. D. Wolchok, Cancer immunotherapy using checkpoint blockade. *Science* **359**, 1350–1355 (2018).
2. J. Larkin *et al.*, Five-year survival with combined nivolumab and ipilimumab in advanced melanoma. *N. Engl. J. Med.* **381**, 1535–1546 (2019).
3. A. Haslam, V. Prasad, Estimation of the percentage of US patients with cancer who are eligible for and respond to checkpoint inhibitor immunotherapy drugs. *JAMA Netw. Open* **2**, e192535 (2019).
4. R. L. Siegel, K. D. Miller, H. E. Fuchs, A. Jemal, Cancer statistics, 2021. *CA Cancer J. Clin.* **71**, 7–33 (2021).
5. H. Sung *et al.*, Global cancer statistics 2020: GLOBOCAN estimates of incidence and mortality worldwide for 36 cancers in 185 countries. *CA Cancer J. Clin.* **71**, 209–249 (2021).
6. L. H. Biller, D. Schrag, Diagnosis and treatment of metastatic colorectal cancer: A review. *JAMA* **325**, 669–685 (2021).
7. M. J. Overman *et al.*, Durable clinical benefit with nivolumab plus ipilimumab in DNA mismatch repair-deficient/microsatellite instability-high metastatic colorectal cancer. *J. Clin. Oncol.* **36**, 773–779 (2018).
8. P. M. Boland, W. W. Ma, Immunotherapy for colorectal cancer. *Cancers (Basel)* **9**, 50 (2017).
9. K. N. Kodumudi *et al.*, Immune checkpoint blockade to improve tumor infiltrating lymphocytes for adoptive cell therapy. *PLoS One* **11**, e0153053 (2016).
10. K. Kim *et al.*, Eradication of metastatic mouse cancers resistant to immune checkpoint blockade by suppression of myeloid-derived cells. *Proc. Natl. Acad. Sci. U.S.A.* **111**, 11774–11779 (2014).

11. J. C. Castle *et al.*, Immunomic, genomic and transcriptomic characterization of CT26 colorectal carcinoma. *BMC Genomics* **15**, 190 (2014).
12. G. Germano *et al.*, Inactivation of DNA repair triggers neoantigen generation and impairs tumour growth. *Nature* **552**, 116–120 (2017).
13. M. Efremova *et al.*, Targeting immune checkpoints potentiates immunoediting and changes the dynamics of tumor evolution. *Nat. Commun.* **9**, 32 (2018).
14. N. N. Rahbari *et al.*, Anti-VEGF therapy induces ECM remodeling and mechanical barriers to therapy in colorectal cancer liver metastases. *Sci. Transl. Med.* **8**, 360ra135 (2016).
15. K. Jung *et al.*, Ly6Clo monocytes drive immunosuppression and confer resistance to anti-VEGFR2 cancer therapy. *J. Clin. Invest.* **127**, 3039–3051 (2017).
16. M. Morimoto-Tomita, Y. Ohashi, A. Matsubara, M. Tsuiji, T. Irimura, Mouse colon carcinoma cells established for high incidence of experimental hepatic metastasis exhibit accelerated and anchorage-independent growth. *Clin. Exp. Metastasis* **22**, 513–521 (2005).
17. N. Pećina-Šlaus, A. Kafka, I. Salamon, A. Bukovac, Mismatch repair pathway, genome stability and cancer. *Front. Mol. Biosci.* **7**, 122 (2020).
18. M. Yarchoan, A. Hopkins, E. M. Jaffee, Tumor mutational burden and response rate to PD-1 inhibition. *N. Engl. J. Med.* **377**, 2500–2501 (2017).
19. J. Duraiswamy, K. M. Kaluza, G. J. Freeman, G. Coukos, Dual blockade of PD-1 and CTLA-4 combined with tumor vaccine effectively restores T-cell rejection function in tumors. *Cancer Res.* **73**, 3591–3603 (2013).
20. K. C. Soares *et al.*, A preclinical murine model of hepatic metastases. *J. Vis. Exp.* **91**, 51677 (2014).
21. E. T. Goddard, J. Fischer, P. Schedin, A portal vein injection model to study liver metastasis of breast cancer. *J. Vis. Exp.* **118**, e54903 (2016).
22. K. Jung *et al.*, Targeting CXCR4-dependent immunosuppressive Ly6C^{low} monocytes improves antiangiogenic therapy in colorectal cancer. *Proc. Natl. Acad. Sci. U.S.A.* **114**, 10455–10460 (2017).
23. S. C. Wei *et al.*, Distinct cellular mechanisms underlie anti-CTLA-4 and anti-PD-1 checkpoint blockade. *Cell* **170**, 1120–1133.e17 (2017).
24. E. Alspach *et al.*, MHC-II neoantigens shape tumour immunity and response to immunotherapy. *Nature* **574**, 696–701 (2019).
25. W. Zou, Regulatory T cells, tumour immunity and immunotherapy. *Nat. Rev. Immunol.* **6**, 295–307 (2006).
26. M. L. Broz *et al.*, Dissecting the tumor myeloid compartment reveals rare activating antigen-presenting cells critical for T cell immunity. *Cancer Cell* **26**, 638–652 (2014).
27. S. Spranger, R. Bao, T. F. Gajewski, Melanoma-intrinsic β-catenin signalling prevents anti-tumour immunity. *Nature* **523**, 231–235 (2015).
28. C. S. Garris *et al.*, Successful anti-PD-1 cancer immunotherapy requires T cell-dendritic cell crosstalk involving the cytokines IFN-γ and IL-12. *Immunity* **49**, 1148–1161.e7 (2018).
29. G. M. Gerhard, R. Bill, M. Messemaker, A. M. Klein, M. J. Pittet, Tumor-infiltrating dendritic cell states are conserved across solid human cancers. *J. Exp. Med.* **218**, e20200264 (2021).
30. E. W. Roberts *et al.*, Critical role for CD103(+)/CD141(+) dendritic cells bearing CCR7 for tumor antigen trafficking and priming of T cell immunity in melanoma. *Cancer Cell* **30**, 324–336 (2016).
31. K. C. Barry *et al.*, A natural killer-dendritic cell axis defines checkpoint therapy-responsive tumor microenvironments. *Nat. Med.* **24**, 1178–1191 (2018).
32. J. P. Böttcher *et al.*, NK cells stimulate recruitment of cDC1 into the tumor microenvironment promoting cancer immune control. *Cell* **172**, 1022–1037.e14 (2018).
33. C. Engblom, C. Pfirschke, M. J. Pittet, The role of myeloid cells in cancer therapies. *Nat. Rev. Cancer* **16**, 447–462 (2016).
34. X. Liu, G. D. Hogg, D. G. DeNardo, Rethinking immune checkpoint blockade: 'Beyond the T cell.' *J. Immunother. Cancer* **9**, e001460 (2021).
35. B. Ruffell, L. M. Coussens, Macrophages and therapeutic resistance in cancer. *Cancer Cell* **27**, 462–472 (2015).
36. J. A. Flores-Toro *et al.*, CCR2 inhibition reduces tumor myeloid cells and unmasks a checkpoint inhibitor effect to slow progression of resistant murine gliomas. *Proc. Natl. Acad. Sci. U.S.A.* **117**, 1129–1138 (2020).
37. J. Yu *et al.*, Liver metastasis restrains immunotherapy efficacy via macrophage-mediated T cell elimination. *Nat. Med.* **27**, 152–164 (2021).
38. S. P. Arlauckas *et al.*, In vivo imaging reveals a tumor-associated macrophage-mediated resistance pathway in anti-PD-1 therapy. *Sci. Transl. Med.* **9**, eaal3604 (2017).
39. C. M. Fares, E. M. Van Allen, C. G. Drake, J. P. Allison, S. Hu-Lieskovan, Mechanisms of resistance to immune checkpoint blockade: Why does checkpoint inhibitor immunotherapy not work for all patients? *Am. Soc. Clin. Oncol. Educ. Book* **39**, 147–164 (2019).
40. J. L. Benci *et al.*, Opposing functions of interferon coordinate adaptive and innate immune responses to cancer immune checkpoint blockade. *Cell* **178**, 933–948.e14 (2019).
41. H. Salmon *et al.*, Expansion and activation of CD103(+) dendritic cell progenitors at the tumor site enhances tumor responses to therapeutic PD-L1 and BRAF inhibition. *Immunity* **44**, 924–938 (2016).
42. S. Hegde *et al.*, Dendritic cell paucity leads to dysfunctional immune surveillance in pancreatic cancer. *Cancer Cell* **37**, 289–307.e9 (2020).
43. M. B. Fuertes *et al.*, Host type I IFN signals are required for antitumor CD8+ T cell responses through CD8α+ dendritic cells. *J. Exp. Med.* **208**, 2005–2016 (2011).
44. A. Gupta *et al.*, Radiotherapy promotes tumor-specific effector CD8+ T cells via dendritic cell activation. *J. Immunol.* **189**, 558–566 (2012).
45. C. Vanpouille-Box *et al.*, DNA exonuclease Trex1 regulates radiotherapy-induced tumour immunogenicity. *Nat. Commun.* **8**, 15618 (2017).
46. A. R. Parikh *et al.*, A phase II study of ipilimumab and nivolumab with radiation in microsatellite stable (MSS) metastatic colorectal adenocarcinoma (mCRC). *J. Clin. Oncol.* **37**, 3514 (2019).
47. P. Charoentong *et al.*, Pan-cancer immunogenomic analyses reveal genotype-immunophenotype relationships and predictors of response to checkpoint blockade. *Cell Rep.* **18**, 248–262 (2017).
48. J. J. Killion, R. Radinsky, I. J. Fidler, Orthotopic models are necessary to predict therapy of transplantable tumors in mice. *Cancer Metastasis Rev.* **17**, 279–284 (1998–1999).
49. K. P. Olive *et al.*, Inhibition of hedgehog signaling enhances delivery of chemotherapy in a mouse model of pancreatic cancer. *Science* **324**, 1457–1461 (2009).
50. D. P. Kodack *et al.*, The brain microenvironment mediates resistance in luminal breast cancer to PI3K inhibition through HER3 activation. *Sci. Transl. Med.* **9**, eaal4682 (2017).
51. S. Jiao *et al.*, Differences in tumor microenvironment dictate T helper lineage polarization and response to immune checkpoint therapy. *Cell* **179**, 1177–1190.e13 (2019).
52. G. B. Ferraro *et al.*, Fatty acid synthesis is required for breast cancer brain metastasis. *Nat. Can.* **2**, 414–428 (2021).
53. A. W. Thomson, P. A. Knolle, Antigen-presenting cell function in the tolerogenic liver environment. *Nat. Rev. Immunol.* **10**, 753–766 (2010).
54. M. Zheng, Z. Tian, Liver-mediated adaptive immune tolerance. *Front. Immunol.* **10**, 2525 (2019).
55. P. J. R. Ebert *et al.*, MAP kinase inhibition promotes T cell and anti-tumor activity in combination with PD-L1 checkpoint blockade. *Immunity* **44**, 609–621 (2016).
56. J. Bendell *et al.*, Efficacy and safety results from IMblaze370, a randomised phase III study comparing atezolizumab+cobimetinib and atezolizumab monotherapy vs regorafenib in chemotherapy-refractory metastatic colorectal cancer. *Ann. Oncol.* **29**, v123 (2018).
57. D. G. Millar *et al.*, Antibody-mediated delivery of viral epitopes to tumors harnesses CMV-specific T cells for cancer therapy. *Nat. Biotechnol.* **38**, 420–425 (2020).
58. E. Maraskovsky *et al.*, Dramatic increase in the numbers of functionally mature dendritic cells in Flt3 ligand-treated mice: Multiple dendritic cell subpopulations identified. *J. Exp. Med.* **184**, 1953–1962 (1996).
59. J. L. Benci *et al.*, Tumor interferon signaling regulates a multigenic resistance program to immune checkpoint blockade. *Cell* **167**, 1540–1554.e12 (2016).
60. A. J. Minn, E. J. Wherry, Combination cancer therapies with immune checkpoint blockade: Convergence on interferon signaling. *Cell* **165**, 272–275 (2016).
61. M. Z. Dewan *et al.*, Fractionated but not single-dose radiotherapy induces an immune-mediated abscopal effect when combined with anti-CTLA-4 antibody. *Clin. Cancer Res.* **15**, 5379–5388 (2009).
62. S. J. Dovedi *et al.*, Acquired resistance to fractionated radiotherapy can be overcome by concurrent PD-L1 blockade. *Cancer Res.* **74**, 5458–5468 (2014).
63. C. Lhuillier, N.-P. Rudqvist, O. Elemento, S. C. Formenti, S. Demaria, Radiation therapy and anti-tumor immunity: Exposing immunogenic mutations to the immune system. *Genome Med.* **11**, 40 (2019).
64. B. A. Tannous, *Gaussia* luciferase reporter assay for monitoring biological processes in culture and in vivo. *Nat. Protoc.* **4**, 582–591 (2009).
65. E. Chung *et al.*, Secreted *Gaussia* luciferase as a biomarker for monitoring tumor progression and treatment response of systemic metastases. *PLoS One* **4**, e8316 (2009).
66. G. B. Lesinski *et al.*, The antitumor effects of IFN-α are abrogated in a STAT1-deficient mouse. *J. Clin. Invest.* **112**, 170–180 (2003).
67. A. M. Bolger, M. Lohse, B. Usadel, Trimmomatic: A flexible trimmer for Illumina sequence data. *Bioinformatics* **30**, 2114–2120 (2014).
68. H. Li, R. Durbin, Fast and accurate short read alignment with Burrows-Wheeler transform. *Bioinformatics* **25**, 1754–1760 (2009).
69. A. McKenna *et al.*, The Genome Analysis Toolkit: A MapReduce framework for analyzing next-generation DNA sequencing data. *Genome Res.* **20**, 1297–1303 (2010).
70. P. Cingolani *et al.*, A program for annotating and predicting the effects of single nucleotide polymorphisms, SnpEff: SNPs in the genome of *Drosophila melanogaster* strain w1118; iso-2; iso-3. *Fly (Austin)* **6**, 80–92 (2012).
71. L. Barbier *et al.*, Two lymph nodes draining the mouse liver are the preferential site of DC migration and T cell activation. *J. Hepatol.* **57**, 352–358 (2012).
72. A. Dobin *et al.*, STAR: Ultrafast universal RNA-seq aligner. *Bioinformatics* **29**, 15–21 (2013).
73. M. Lawrence *et al.*, Software for computing and annotating genomic ranges. *PLoS Comput. Biol.* **9**, e1003118 (2013).
74. M. I. Love, W. Huber, S. Anders, Moderated estimation of fold change and dispersion for RNA-seq data with DESeq2. *Genome Biol.* **15**, 550 (2014).
75. A. Subramanian *et al.*, Gene set enrichment analysis: A knowledge-based approach for interpreting genome-wide expression profiles. *Proc. Natl. Acad. Sci. U.S.A.* **102**, 15545–15550 (2005).
76. V. K. Mootha *et al.*, PGC-1α-responsive genes involved in oxidative phosphorylation are coordinately downregulated in human diabetes. *Nat. Genet.* **34**, 267–273 (2003).
77. Y. Shen *et al.*, Reduction of liver metastasis stiffness improves response to bevacizumab in metastatic colorectal cancer. *Cancer Cell* **37**, 800–817.e7 (2020).
78. V. Palmieri *et al.*, Neutrophils expressing lysyl oxidase-like 4 protein are present in colorectal cancer liver metastases resistant to anti-angiogenic therapy. *J. Pathol.* **251**, 213–223 (2020).
79. S. Hänzelmann, R. Castelo, J. Guinney, GSVA: Gene set variation analysis for microarray and RNA-seq data. *BMC Bioinformatics* **14**, 7 (2013).
80. W. Li *et al.*, Combining losartan with radiotherapy increases tumor control and inhibits lung metastases from a HER2/neu-positive orthotopic breast cancer model. *Radiat. Oncol.* **16**, 48 (2021).